EXPERIMENTAL CHARACTERIZATION OF CREEP DAMAGE USING THE NONLINEARITY ULTRASONIC TECHNIQUE

A Thesis
Presented to
The Academic Faculty

by

Christian Ehrlich

In Partial Fulfillment
of the Requirements for the Degree
Master of Science in
Engineering Science and Mechanics

School of Civil and Environmental Engineering
Georgia Institute of Technology
December 2011

EXPERIMENTAL CHARACTERIZATION OF CREEP DAMAGE USING THE NONLINEARITY ULTRASONIC TECHNIQUE

Approved by:

Dr. Laurence J. Jacobs, Advisor
School of Civil and Environmental Engineering
Georgia Institute of Technology

Dr. Jin-Yeon Kim
George W. Woodruff School of Mechanical Engineering
Georgia Institute of Technology

Dr. Jianmin Qu
School of Civil and Environmental Engineering
Northwestern University

Date Approved: August 2011

ACKNOWLEDGEMENTS

First of all, I would like to thank my advisor Dr. Laurence J. Jacobs who made my stay in Atlanta possible at all. Throughout this project he was extremely supportive and never seized to encourage me. He also gave me the opportunity to present my research at QNDE 2011 in Burlington.

I want to thank Dr. Jin-Yeon Kim for helping me with every aspect of my thesis in the most outstanding way. His sharp intellect and great personality were not only fundamental to this work but also made working with him a great experience.

I thank Dr. James Wall for providing me with the creep specimen and advice and help in many topics. Furthermore I want to thank Dr. Jianmin Qu for being part of my committee and for his helpful advice. Moreover I want to express my gratitude to Dr. Kimberly E. Kurtis and Dr. Preet Singh for letting me use their equipment.

I want to thank the Institute of Applied Mechanics of the University of Stuttgart. In particular I thank Dr. Lothar Gaul for choosing me to participate in the ISAP program and for creating and maintaining the program in the first place. Furthermore I am very grateful to Dr. Helge Sprenger and Dipl.-Ing Jan Herrmann for organizing the exchange program and dedicating a lot of time to help me before and during my stay in Atlanta. The financial support of the DAAD is also greatly appreciated.

I want to express my deep gratitude to my friend in Germany for staying in contact with me and to my friends in Atlanta for sharing many great experiences with me.

I especially thank my labmates Yu Liu, Katie Matlack, Simon Walker and Matthias Seher for making work always pleasant. Most importantly I thank my family for their love and support.

TABLE OF CONTENTS

LIST OF TABLES

LIST OF FIGURES

LIST OF SYMBOLS

Symbol	Description
a	Area under the Transducer
$a(\omega)$	Attenuation Loss Factor
A	Displacement Amplitude
A_1	Fundamental Amplitude
A_2	Second Harmonic Amplitude
c	Velocity
c_L	Phase Velocity of Longitudinal Wave
c_T	Phase Velocity of Shear Wave
C_{ijkl}	Second Order Elastic Constant
C_{ijklmn}	Third Order Elastic Constant
$\mathbf{d}$	Direction of Particle Movement
D	Diffraction Loss
E_{ij}	Lagrangian Strain Tensor
f	Frequency
$\mathbf{f}$	Body Force
F	Force Amplitude
F_{ij}	Deformation Gradient Tensor
H	Transfer Function
i	Imaginary Unit
I	Current
k	Wave Number
K	Conversion Efficiency
$\mathbf{n}$	Normal Vector
$\mathbf{p}$	Direction of Wave Propagation

Symbol	Description
P_A	Acoustical Energy
P_E	Electrical Energy
P_ij	Piola-Kirchhoff Stress
S	Surface
t	Time
$\mathbf{t}$	Traction
$\mathbf{u}$	Displacement
V	Volume, Voltage
W	Strain Energy
x	Propagation Distance
X_j	Langrangian Coordinate
Z	Impedance
β	Material Nonlinearity Parameter
δ_{ij}	Kronecker Delta
ϵ_{ij}	Strain Tensor
Θ	Angle of Incident/ Reflected Wave
λ, μ	Lamé Constants
ρ	Density
σ_{ij}	Stress Tensor
ϕ	Scalar Potential
$\mathbf{\Phi}$	Vector Potential
ω	Angular Frequency
∇	Differential Operator

SUMMARY

Welded steel pipes are an essential structural part of any power plant. Longer lifetimes and higher pressures in the pipes cause an increased probability of failure due to creep damage. To maintain safe operation, nondestructive evaluation techniques to detect creep damage are needed. Nonlinear acoustic techniques employing longitudinal waves have been proven to be sensitive to creep damage. The objective of this research is to develop a robust experimental procedure to reliably measure the acoustic nonlinearity parameter using longitudinal waves, and then to validate the procedure on samples of different materials and sizes. Finally the technique is applied to characterize creep damage levels around the weld of a welded steel pipe. While the experimental technique presented can only measure the relative nonlinearity, it is accurate enough to detect changes in nonlinearity due to creep damage. Measurements show an increase in nonlinearity in the heat affected zone (HAZ). Experiments after annealing the creep damaged specimen show a decrease in nonlinearity in accordance with a decrease in dislocation density. Measurements on an undamaged welded A36 steel component suggest that the heat itself is not responsible for the increase in nonlinearity.

CHAPTER I

INTRODUCTION

1.1 Motivation

In order to operate a power plant in an economical and environmentally friendly way, it is important to ensure safety and simultaneously extend the lifetime of the power plant as much as possible. Furthermore, in an effort to increase efficiency, modern power plants operate under very high steam pressure. The stresses under high temperature and pressure cause creep in structural parts such as pipes which over their long lifetime, can cause failure of the part. This is not only an economical threat due to possible down-times and high repair costs, but it also poses a direct threat to people working in the environment of power plants. To ensure a safe and long operation, nondestructive evaluation (NDE) techniques are necessary to monitor structural components. This is especially true for the welds, because the welds are where a majority of failures occur. A promising approach for NDE on steel pipes is nonlinear ultrasonics because previous research has already demonstrated a strong correlation between creep damage and material nonlinearity [17]. Creep damage in welded steel pipes is localized and usually occurs within the structure, not on the surface. Longitudinal waves can interrogate small volumes but through the full depth of a component which makes them very well suited to track changes in localized damage.

1.2 Literature Review

Nonlinear ultrasonic techniques have attracted growing attention. An extensive review of the theoretical groundwork is given by Hamilton in [8]. Dace et al. present the

theory of how to calibrate transducers for absolute measurements in [6]. In [7] they prove the capability of nonlinear ultrasonic techniques in the through transmission mode to obtain accurate absolute material nonlinearity parameters. Earlier measurements of absolute material nonlinearity have been done by Thompson et al. in [18]. While the first applications of nonlinear ultrasonic techniques were predominantly used to quantify fatigue damage, more recent research shows similar potential for creep damage. An extensive review of linear and nonlinear techniques to detect creep damage is given by Sposito [17]. Baby et al. used contact transducers for nonlinearity measurements tracking creep damage in titanium alloy. Their results presented in [2] suggest that the third harmonic as an even more sensitive measure of creep damage. Ohtani et al. presents a nonlinear technique employing non-contact electromagnetic acoustic transducers (EMATs) to asses creep damage in welded boiler heat exchange tubes with special focus on the heat affected zone in [13]. A good correlation between nonlinear testing results and microscopic evaluation of the micro-structure was found.

1.3 Objective

The objective of this research is to develop a robust experimental procedure to reliably measure the absolute material nonlinearity parameter using longitudinal waves, validate the procedure with measurements on samples of different sizes and materials and finally use the procedure for nonlinear measurements on a welded steel pipe component, comparing damage levels in the heat affected zone and the base material.

1.4 Structure of this Thesis

This thesis begins with a brief theoretical background. Starting from the balance of momentum, the basic ideas of linear and nonlinear wave propagation are developed. The theoretical part of this thesis also includes an overview of the development and characteristics of creep damage.

The next chapter introduces the experimental setup. Because the technique developed

contains of two separate measurements, the calibration and the nonlinear measurement, that share some equipment, this chapter is divided in two parts. First the complete instrumentation is presented in detail followed by a discussion on how each part of the instrumentation meets the needs of the measurement. Then the experimental procedures of calibration and nonlinear measurement are presented. During the course of this research the measurement setups have been improved. This chapter only presents the setup that is found to have the best performance.

The results chapter presents the findings of this project. It starts with an evaluation of the calibration measurement. Then different aspects of the nonlinear measurement concerning the setup and the performance are presented. After that the results of the nonlinear measurements on creep damaged specimen are given together with the results of additional measurements that help to put the data from the creep specimens into the right context.

The last chapter includes conclusions that can be derived from this research and gives an outlook on possible future work.

CHAPTER II

THEORY

2.1 Wave Propagation

This chapter gives a brief overview of the theoretical basis of this work. Various mathematical formulations that are helpful to solve wave propagation problems related to the focus of this research are derived. First the general equations of motion in a linear, isotropic material in terms of the displacement are derived. Then the focus will be narrowed down to plane harmonic waves propagating in linear elastic media. In the last part of this chapter the assumption of the linear elasticity is dropped and the basic ideas of nonlinear wave propagation are presented.

Most of the equations in this chapter are defined in three dimensional space. Sometimes it is easier to write those equations in terms of vectors whereas in other cases index notation is more advantageous. In order to make those two different notations easy to distinguish, vectors will be denoted with bold letters, e.g. $\mathbf{u}$ and variables in index notation will be denoted with regular letters plus subscript as in u_i.

2.1.1 Equation of Motion

A comprehensive derivation of the equations of motion and a good introduction to linear wave propagation in general can be found in [1]. Here only a short introduction is given. In order to understand the physical and mathematical background governing the propagation of waves one can start with the balance of linear momentum for a body with volume V and surface S which is subject to a traction t_i on its surface as well as a body force f_i:

$$\int_S t_i \mathrm{d}S \; + \int_V \rho f_i \mathrm{d}S \; = \int_V \rho \ddot{u}_i \, \mathrm{d}V \tag{2.1}$$

Where ρ is the density and u_i the i-th component of the displacement vector. With the help of the Cauchy stress formula

$$t_i \;=\; \sigma_{ij} n_j, \tag{2.2}$$

with σ_{ij} being the stress tensor and n_i the i-th component of the outward normal vector and applying Gauss' theorem, the balance of linear momentum can be transformed to

$$\int_V (\sigma_{ij,j} \;+\; \rho f_i \;-\; \rho \ddot{u}_i) \;=\; 0. \tag{2.3}$$

This equation must hold for any arbitrary portion of the volume (Localization Argument). Therefore it can be simplified to the Cauchy's equation of motion

$$\sigma_{ij,j} \;+\; \rho f_i \;-\; \rho \ddot{u}_i \;=\; 0. \tag{2.4}$$

For the rest of the thesis the body force f_i will be neglected. The Cauchy's equation of motion can be further modified in order to obtain equations that only depend on the displacement and material constants. For that purpose it is useful to first assume a linear, homogeneous, isotropic material. In that case strain ϵ_{ij} and stress σ_{ij} are related by Hooke's law:

$$\sigma_{ij} \;=\; \lambda \delta_{ij} \epsilon_{kk} \;+\; 2\mu \epsilon_{ij}, \tag{2.5}$$

where μ and λ are the Lamé constants. The strain is defined by

$$\epsilon_{ij} = \frac{1}{2}(u_{i,j} \;+\; u_{j,i}). \tag{2.6}$$

Using Equations (2.6) and (2.5) to eliminate σ_{ij} in Equation (2.4) and keeping in mind that the body force f_i is neglected, one arrives at the Navier equations

$$(\lambda \;+\; \mu) u_{j,ji} \;+\; \mu u_{i,jj} \;=\; \rho \ddot{u}_i \tag{2.7}$$

or in vector representation

$$\mu \nabla^2 \mathbf{u} \;+\; (\lambda \;+\; \mu) \nabla \nabla \cdot \mathbf{u} \;=\; \rho \ddot{\mathbf{u}}. \tag{2.8}$$

This represents a system of three coupled partial differential equations. While one dimensional wave propagation problems can be solved directly from this set of equations, more complex problems can only be solved assuming potentials and applying the Helmholtz decomposition. In terms of the scalar potential ϕ and the vector potential $\mathbf{\Phi}$, the displacement is given as

$$\mathbf{u} \;=\; \nabla\phi \;+\; \nabla \times \mathbf{\Phi}. \tag{2.9}$$

In order to also guarantee uniqueness of the solution

$$\nabla \cdot \mathbf{\Phi} \;=\; 0, \tag{2.10}$$

has to be satisfied. Substituting Equation(2.10) into Equation (2.7) finally yields two uncoupled equations in terms of ϕ and $\mathbf{\Phi}$:

$$(\lambda \;+\; 2\mu)\nabla^2\phi \;=\; \rho\ddot{\phi} \tag{2.11}$$

$$\mu\nabla\mathbf{\Phi} \;=\; \rho\ddot{\mathbf{\Phi}} \tag{2.12}$$

2.1.2 Linear Wave Propagation

2.1.2.1 Plane Waves

A wave whose planes of constant phase are normal to the direction of propagation $\mathbf{p}$ is called a plane wave. While it is technically not possible to generate such a wave it is a good approximation for many waves, among them are longitudinal waves from a transducer with a flat face which are employed in this research. The advantage of this approximation is that many phenomena of wave propagation can be expressed fairly easy for plane waves. Thus the derivations in this chapter are all based on the assumption of plane waves. Mathematically the displacement in an elastic solid due to a plane wave that propagates with the velocity c in the direction of the unit vector $\mathbf{p}$ can be expressed as

$$\mathbf{u} \;=\; f(\mathbf{x} \cdot \mathbf{p} \;-\; ct)\mathbf{d}. \tag{2.13}$$

Substituting this formula into Equation (2.8) yields

$$(\mu \ - \rho c^2)\mathbf{d} \ + \ (\lambda \ + \ \mu)(\mathbf{p} \cdot \mathbf{d}) \ = \ 0. \tag{2.14}$$

This equation can only be satisfied in two distinct cases.

1. $\mathbf{d} \ = \ \pm\mathbf{p}$, which means that direction of particle movement and the direction of propagation are parallel. This case is called a longitudinal wave or P-wave. In this case Equation (2.14) yields

$$c \ = \ c_L \ = \ \left(\frac{\lambda \ + \ 2\mu}{\rho}\right)^2; \tag{2.15}$$

2. $\mathbf{p} \ \cdot \mathbf{d} \ = \ 0$, which means that direction of particle movement and the direction of propagation are perpendicular. This case is called a shear wave. If the wave propagates in a two-dimensional plane it can either have an in-plane displacement (SV-wave) or and out-of-plane displacement (SH-wave). In both cases Equation (2.14) yields

$$c \ = \ c_T \ = \ \left(\frac{\mu}{\rho}\right)^2. \tag{2.16}$$

In is noteworthy that $c_L \ > c_T$ always holds. The longitudinal wave therefore always propagates faster than the shear wave.

A special case of plane waves are time harmonic plane waves for which the original Equation for the displacement (2.13) written as

$$\mathbf{u} \ = \ A\,\mathbf{d}\exp[i\,k(\mathbf{x} \cdot \mathbf{p} \ - \ c\,t)], \tag{2.17}$$

where A is the (complex) amplitude of the wave and $k = \frac{\omega}{c}$ the wave-number. $\omega \ = 2\pi f$ is the angular frequency. It is important to note that A depends neither on x nor on t.

2.1.2.2 Reflection of longitudinal waves

So far only an infinite medium without any discontinuities has been considered in order to derive wave speeds and displacements. If however the medium has discontinuities, new phenomena arise. At an arbitrary interface between two layers reflection

and transmission occur. The most important case for this research however is the interface between a metallic medium (test-sample) and air - a so-called free boundary. The acoustic impedance of the metallic medium is much higher than the acoustic impedance of air. Therefore almost no energy will be transmitted and refraction can be neglected. An incident P-wave that is reflected at a free boundary generally creates P- and SV-waves. The angle under which the reflected waves propagate depends on the angle of the incident wave Θ_0. In particular, if $\Theta_0 = 0$ there is no reflected SV-wave.

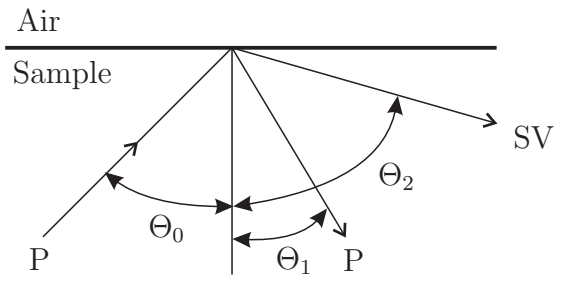

Figure 2.1: Reflection of a P-wave at a free boundary.

In this research the transducers will always be placed on two opposing parallel surfaces and only generate P-waves. Thus only P-waves will be present within structure. For SV-waves similar relations for the generation of reflected SV- and P-waves can be obtained. An incident SH-wave on the other hand cannot generate any other types of waves.

Table 2.1: Angle relations for reflection at a free boundary.

incident P-wave	reflected P-wave	reflected SV-wave
Θ_0	$\Theta_1 = \Theta_0$	$\sin\Theta_2 = \sin(c_T/c_L)\sin\Theta_0$

2.1.3 Nonlinear Wave Propagation

Even though in the majority of cases the linear wave theory is sufficient, nonlinear approaches are necessary sometimes. One of this cases is the use of nonlinear acoustics for nondestructive evaluation which is used in this thesis. Especially the generation of higher harmonics through material nonlinearity is of interest. This means that assuming a nonlinear material, a pure wave of frequency ω gets distorted as it travels through the material. Therefore at the output, the signal does not only contain portions with the frequency ω but also higher harmonics with frequencies that are integer multiples of ω.

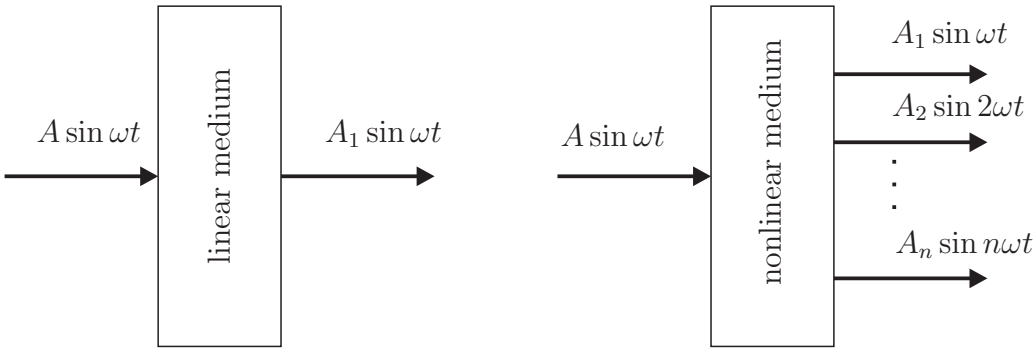

Figure 2.2: Linear and Nonlinear Wave Propagation.

As with the linear case only a short overview of the derivation shall be given here. A more detailed explanation can be found in [8]. The derivation of nonlinear wave equations is commonly done in Lagrangian coordinates. This coordinate frame is denoted by X. The relation between Eulerian coordinates, denoted with x, and Langrangian coordinates is defined to be

$$F_{ij} \;=\; \frac{\partial x_i}{\partial X_j}, \tag{2.18}$$

the deformation gradient tensor. The starting point for the further derivation is the balance of linear momentum in Langrangian coordinates,

$$\rho_0 \frac{\partial^2 u_i}{\partial t^2} \;=\; P_{ij,j}, \tag{2.19}$$

where ρ_0 denotes the density in the initial configuration and P_{ij} is the Piola-Kirchhoff stress. The Piola-Kirchhoff stress can be expressed in terms of strain energy W as follows:

$$P_{ij} \;=\; \rho_0 \,\mathbf{F}\, \frac{\partial W}{\partial \mathbf{E}}, \tag{2.20}$$

with

$$E_{ij} \;=\; \frac{1}{2}\left(\frac{\partial u_i}{\partial X_j} \;+\; \frac{\partial u_j}{\partial X_i} \;+\; \frac{\partial u}{X_i}\,\frac{\partial u_j}{\partial X_i}\right), \tag{2.21}$$

the Lagrangian strain tensor. For small strains one can assume a power series expansion for the strain Energy

$$\rho_0 W \;=\; \frac{1}{2!} C_{ijkl} E_{ij} E_{kl} \;+\; \frac{1}{3!} C_{ijklmn} E_{ij} E_{kl} E_{mn} \;+\; \ldots \tag{2.22}$$

with C_{ijkl} and C_{ijklmn} being the second and third order elastic constants respectively. Putting together Equations (2.19) - (2.22) yields a nonlinear differential equation for the displacement which in the case of a one dimensional wave can be written as

$$\frac{\partial^2 u}{\partial t^2} \;=\; {c_L}^2 \frac{\partial^2 u}{\partial X^2}\left(1 \;-\; \beta^2 \frac{\partial u}{\partial X}\right), \tag{2.23}$$

where β is the material nonlinearity parameter defined by

$$\beta \;=\; -\left(\frac{3}{2} \;+\; \frac{C_{111111}}{2\rho {c_L}^2}\right). \tag{2.24}$$

The solution of the nonlinear wave equation in case of harmonic excitation is

$$u \;=\; \underbrace{u_0}_{A_1} \sin(\omega t \;-\; kx) \;+\; \underbrace{\frac{\beta}{8}\left(\frac{\omega u_o}{c_L}\right)^2 x}_{A_2} \sin(2\omega t \;-\; 2kx). \tag{2.25}$$

This yields the following expression for β

$$\beta \;=\; \frac{8 A_2 {c_L}^2}{\omega^2 {A_1}^2 x} \tag{2.26}$$

Obviously, if one measures the longitudinal wave speed, the fundamental amplitude A_1 and the second harmonic A_2, β can be calculated. Besides this experimental approach, the theoretical value of β can be calculated according to Equation 2.24. Conversely, from the measured β, one can calculate the third order elastic constant C_{111111}.

2.2 Creep

Time dependent plasticity of materials under high temperature is generally denoted by the term creep. There are many extensive reviews of creep mechanisms for example in [10] and [11]. For this project creep under a constant stress is of major interest. It is important to note that creep occurs even if the applied stress is much lower than the room-temperature yield stress. Under this conditions one can identify three different stages of creep life characterized by a curve of strain vs. time as in Figure 2.3. The first reaction of the material to a load is instantaneous strain deformation followed by a decrease of the strain rate (Stage I). After that a long period of constant strain rate follows (Stage II) until the strain rate accelerates again, eventually causing rupture (Stage III). The changes in strain rate from stage to stage are caused by a variety of mechanisms including strain hardening, recovery precipitation of carbides, cavity formation and others [17]. The dominante mechanism however is dislocation motion with diffusion of vacancies [4]. These mechanisms eventually lead to crack initiation. Cracks can grow and propagate very quickly. Therefore early damage detection is a paramount safety concern.

Dislocations and voids are a source of nonlinearity which can increase the material

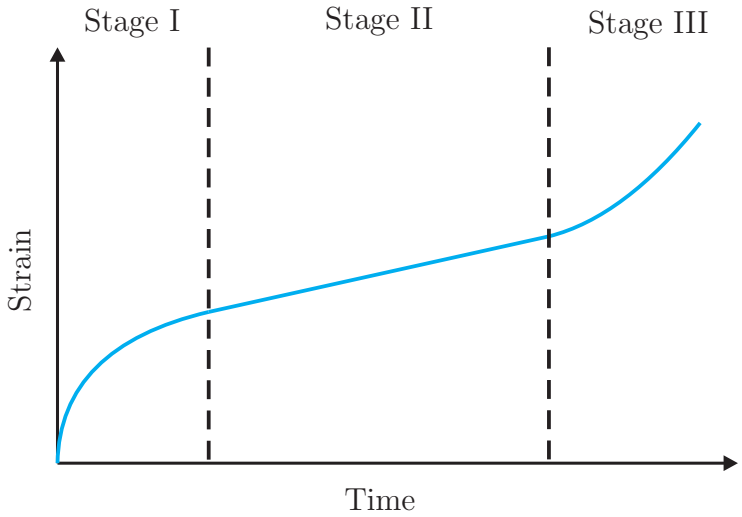

Figure 2.3: Stages of Creep Life.

nonlinearity parameter. Therefore nonlinear ultrasonic techniques are capable of detecting creep damage even at an early stage.

The structures of interest for this project are welded steel pipes. Creep damage in those structures is usually associated with the weld. Figure 2.4 shows a typical weld consisting of three zones: the base material, the heat affected zone (HAZ), and the weld [13]. The HAZ is a transition zone that typically can further be divided into a coarse grained zone next to the weld and a fine grained zone adjacent to the base material. All these zones have different creep properties which generate a highly complicated behavior with a variety of failure mechanisms. In ferritic steel pipes in long term service however, failure mostly occurs in the HAZ. The predominant type of damage is called a Type IV damage. It is caused by a large difference of creep resistance of the fine grained zone in the HAZ (low creep resistance) and the base material (high creep resistance). The damage usually occurs in the interior of the interface as shown in Figure 2.4, where the stress rate is more complex than on the surface. A nondestructive technique to monitor this kind of damage therefore must be able to examine the full depth of the structure.

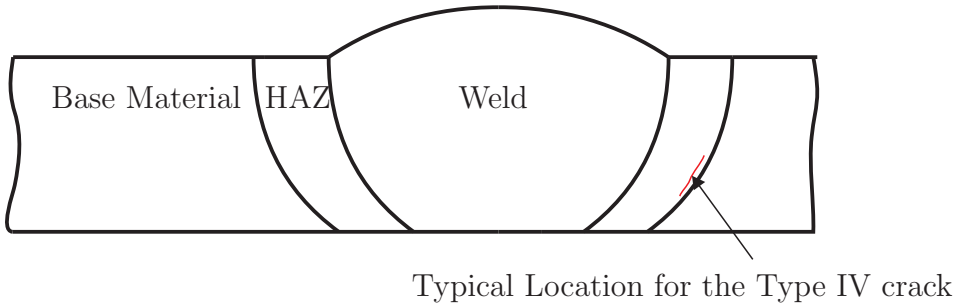

Figure 2.4: Weld Showing the Three Different Zones and Type IV Damage.

CHAPTER III

EXPERIMENTAL SETUP

Nonlinear acoustic techniques are highly sensitive to influences, specifically the inherent nonlinearity of the used equipment. Therefore each part must be chosen carefully and its influence on the measurements should be evaluated. In order to find a precise and reliable experimental setup many different options were considered. In this chapter all parts that are to obtain the nonlinear acoustic measurements are described and evaluated in terms of fulfilling their particular requirements.

3.1 Pulser

The nonlinear technique used in this research requires a calibration of the receiving transducer in order to convert measured voltages to physical displacements and to account for changes in the coupling condition between the receiver and the sample. The calibration is done according to the procedure presented in [7] which employs a broadband pulser. The requirements for this piece of equipment are not very specific and most available pulsers can be used. Merely the input impedance must be known and ideally be adjustable. Furthermore the pulse height should be as sufficiently high because the calibration depends on the measurement of the free back wall reflection which is easier if the incident pulse is strong. In this research two different pulsers were used depending on availability:

1. The Panametrics 5072 PR with an available pulse voltage up to 360 V and an adjustable input impedance between 15 and 500 Ohms

2. The Olympus 5058 PR with an available pulse voltage up to 900 V and an adjustable input impedance between 50 and 500 Ohms

Both satisfy all needs for the calibration and deliver similar results.

3.2 Equipment to Generate Input Signal

For the nonlinear measurements, short high power toneburst signals are used. In order to be able to measure material nonlinearity, it is crucial that the original signal is as clean as possible. This means that ideally the signal should only contain a single frequency. The following section presents the equipment that is used to achieve that.

3.2.1 RITEC RAM-5000

The main requirement for the generated signal besides the aforementioned purity is a high power output. In metallic materials the nonlinearity is relatively small which means that the amplitude of the second harmonic is much smaller than the amplitude of the fundamental. Therefore it is essential to have a high power input signal in order to detect the second harmonic and to have a reasonable signal to noise ration (SNR). Also the material nonlinearity parameter is higher at low amplitudes and decreases quickly until a certain input level is reached. Only for higher excitation the nonlinearity parameter converges to a constant value [21]. The RITEC RAM-5000 is specifically designed for those needs typical in applications of nonlinear ultrasonic measurements. It generates a clean output signal and can deliver power outputs up to 1.5 kW RMS. Further specifications can be found in Table 3.1.

Table 3.1: Specifications RITEC RAM-5000.

Typical Gated Amplifier RMS Output	1.5 KW between 0.25 and 7 Mhz
Frequency Range for Gated Amplifier	250 kHz to 17.5 MHz
Nominal Output Impedance of Gated Amplifier	50 Ohms
Maximum Pulse Width	200 microseconds

3.2.2 RITEC FD-5-10 Low-Pass Filter

Even though the RITEC RAM-5000 is specifically designed to generate pure signals, an additional Low Pass Filter (LPF) can still reduce the amplitude of unwanted higher harmonics significantly and is therefore an important part of the experimental setup. The FD-5-10 is a system that contains a 5 MHz Low Pass Filter and a 10 MHz High Pass Filter (HPF). The LPF is a Chebyshev filter with 50 Ohm input impedance matching the output impedance of the amplifier and 200 MHz output impedance which is an approximation of the impedance of a piezoelectric transducer. The matching of the impedances is important in order to avoid an impedance mismatch which could distort the signal [9]. The HPF of the FD-5-10 system can be used to measure the second harmonic. In this research it is only used to validate the results of the signal processing.

3.2.3 RITEC RA-6 High Power Attenuator

A 6dB attenuator is placed between amplifier and filter. Its main purpose is to improve the impedance matching between the filter and the amplifier by providing a more constant output impedance than the amplifier. The attenuator obviously reduces the peak output power that can be delivered to the transducer; therefore, one has to omit the attenuator if higher output levels are necessary in applications such as very large samples or if a transducer with a low power conversion efficiency is used. Even though both, filter and attenuator, reduce the signal strength, they should always be included if possible because the quality of the signal gets improved drastically. Figure 3.1 shows the second harmonic of the signal straight after the amplifier and after attenuator and filter. For both measurements, the amplifier output signal is a 30 cycle 5 MHz toneburst at 95 % output level. The recorded signals are then normalized with respect to their fundamental frequency peak.

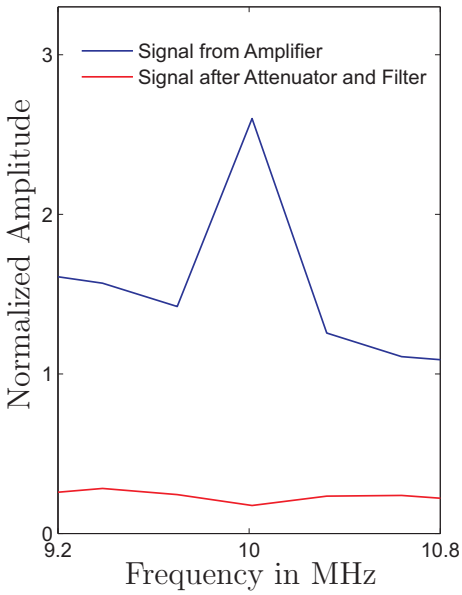

Figure 3.1: Comparison between Second Harmonic of Signal from Amplifier and Signal after Attenuator and Filter.

It is clearly visible that the second harmonic portions of the signal are successfully filtered out by the LPF. The amplitude of the second harmonic gets reduced by a factor of 148 and the ratio of the fundamental to the second harmonic gets increased to 76dB from 46dB without filter and attenuator.

3.3 Transducers

Figure 3.2: Valpey Fisher 5MHz and 10MHz $LiNbO_3$ transducers.

The transducers convert the electrical signal into a mechanical wave and then

back and are therefore one of the most important pieces of equipment. Even an absolutely clean electrical input signal would be worthless if the transducers are not linear and distort the signal significantly. This means that the transducer itself should not generate any higher harmonics. Furthermore, the transmitting transducer should be reasonably efficient which means that it should convert as much electrical energy to mechanical energy as possible. The receiver should obviously do the same in the opposite direction. The electrical input signal for the transducer in this research is a 5 MHz toneburst. Therefore the transducer has its eigenfrequency exactly at this point. Since this research is specifically interested in the generation of second harmonics, the receiving transducer has its eigenfrequency at 10 MHz, which is twice the eigenfrequency of the transmitter.

In this research only piezo-electric contact transducers are used. They are readily available and generally easy to handle. Transducers based on Lithim-Niobate ($LiNbO_3$) are generally more linear than PZT-based transducers and therefore used in this research. More details to the properties of $LiNbO_3$ transducers can be found in [22]. For the measurements, three different types of $LiNbO_3$ based transducers were used each of which has different advantages.

1. Standard Transducers with backing
2. Custom Made Transducers without Backing
3. Crystal Transducer

3.3.1 Standard Transducer

The standard transducers used in this research are made by Valpey Fisher. Both 5 MHz transmitter and 10 MHz receiver are 0.5 inches in diameter. The advantages of these transducers is the commercial availability and the easy fluid coupling to the sample. This means that the transducers can simply be pressed onto the sample

with a thin layer of fluid couplant on its surface. Furthermore the output of the transmitter, if used with the RITEC amplifier, attenuator, and filter, is high enough to reach the level of constant material nonlinearity. However these transducers are not absolutely linear. The $LiNbO_3$ crystal itself is known to be very linear, therefore other influences must account for the extra nonlinearity. A possible cause for extra nonlinearity is the backing of the transducer. It exists to reduce ringing and to make the transducer more durable. But energy transfer between the crystal and the backing can possibly cause distortion.

3.3.2 Custom Made Transducer

In order to eliminate the backing as potential source of nonlinearities custom transducers have been manufactured by Valpey Fisher. Those transducers are for the most parts equivalent to the commercial transducers but have no backing. The casing still offers the possibility of fluid coupling but without backing the transducers are fragile and less force can be exerted on them to press them against the sample. On the other hand energy dissipation is reduced which means higher output levels can be achieved. A comparison in terms of linearity of commercial and custom transducers can be found in Chapter 4.

3.3.3 Crystal Transducer

The pure $LiNbO_3$ crystal is known to be very linear. Moreover it is more efficient in converting the electrical signal into a mechanical signal than the cased transducers because no energy can be dissipated by any casing or backing. These advantages are opposed by a very problematic handling. The crystals are very fragile. Therefore only little force can be exerted on them which means that simple fluid coupling is hard to realize. Therefore other options like glue or Salol bonding have to be used. Thus the preparation for the measurement is much more complicated than with cased transducers. Especially removing the crystals from the sample after they have been

glued can take a lot of time and care. But even if great care is taken when the crystals are handled, it is hard to avoid breaking them eventually if they are used frequently. Therefore those transducers are not a viable solution for everyday measurements. Their superior output behavior makes them a good choice to obtain bottom line measurements and evaluate other transducers.

3.4 Fixture

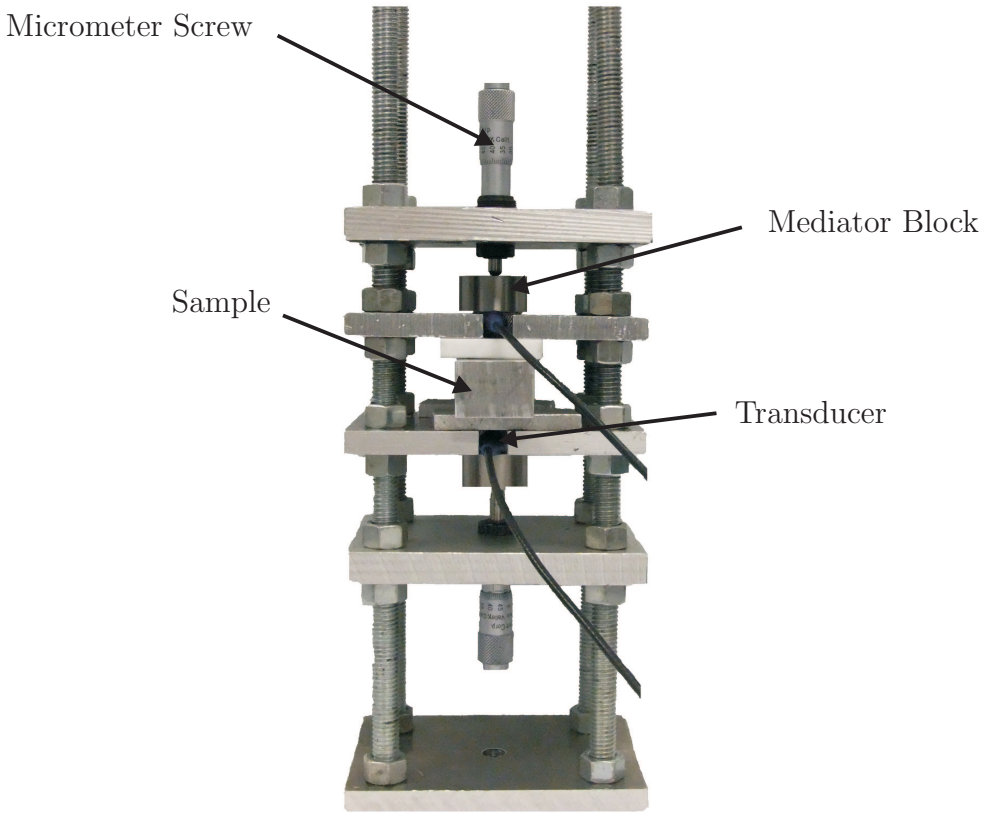

Figure 3.3: Fixture.

The used measurement method requires that the transducers can be attached independently without changing the bonding situation for the other transducer respectively. Furthermore both transducers need to be placed exactly opposite of each

other on both sides of the sample. Both requirements are fulfilled by the fixture shown in Figure 3.3 . In order to facilitate repeatable measurements micrometer screws are used to exert a force on small pads that rest on the transducers. This way for each measurement the same force can be applied to the transducer. This fixture is adaptable to samples that do not exceed the distance between the outer screws (60 mm) or maximum available height (130mm). The minimum size of a sample is dictated by the size of the transducers.

3.5 Measurement Equipment

Because the amplitude of the second harmonic is relatively small compared to the original amplitude, it is very important to have precise measurement equipment. For the calibration, current and voltage signals have to be recorded. For the nonlinearity measurement, only the current needs to be recorded. This means in total a current probe, a voltage probe and an oscilloscope are needed for data aquisition.

3.5.1 Current Probe Tektronix P6021

The Tektronix P6021 current probe is designed for AC currents up to 15 A in a frequency range from 120 Hz to 60Mhz. These specifications exceed the anticipated range that is necessary for the measurement by far. Therefore the probe is a viable choice.

3.5.2 Voltage Probe Tektronix P5050

The passive voltage probe P5050 allows 300 V CAT II input voltage and frequencies up to 500 MHz. This also satisfies all requirements for the voltage probe in this research.

3.5.3 Oscilloscope Tektronix TDS 420

The highest frequency of interest in this research is 10 MHz. In order to avoid aliasing and ensure a perfect reconstruction of the signal the sampling frequency has

to be at least twice as high, in this case 20 MHz. This is therefore the minimum requirement for the oscilloscope. Furthermore it has to have at least three inputs in order to measure voltage and current signals at the same time and also connect the synchronization from the pulser. The TDS 420 has four input channels and can sample all of them at the same time at up to 100 MS/s (100 MHz). The record length can be varied between 500 to 15,000 points depending on the desired sampling frequency and time period.

3.6 Calibration Procedure

3.6.1 Theoretical Background

Each measurement begins with the calibration of the receiving transducer. That way, the electrical signal from the receiver can be converted into actual displacements in the next step. Furthermore, the calibration accounts for changes in the coupling situation of the transducer, specifically the thickness of the couplant layer which has a great influence on the transmission. The calibration method used in this project is presented in great detail in [6] and [7]. The goal of this calibration is to determine the transfer function between the mechanical signal (displacement) and the electrical signal. In order to do so one can examine the impulse-response of the receiving transducer. This technique only works if the transducer is reciprocal, because the signal passes through it twice in opposite directions. The reciprocity can be proven using the two port model of the calibration setup presented in Figure 3.4. The pulser is substituted by the source voltage V_s and the source impedance Z_s. This gives rise to the input voltage V_{in} and the input current I_{in} to the transducer in transmitting mode represented by the two-port. The output of the transducer is a force of amplitude F_{in} with the velocity of amplitude u_{in}. The next two-port is a model of the sample that includes the diffraction loss $D(x, \omega)$ and attenuation $\alpha(\omega)$. Therefore the signal that comes back to the transducer after reflection at the free boundary is changed to

F_{out} and u_{out}. In this work, attenuation will not be accounted for because the test samples are very thin, resulting in a low attenuation. The diffraction loss will be addressed with a diffraction correction according to [15]. After the reflection at the free boundary, the signal arrives back at the transducer which is in receiving mode this time. The acoustic wave gets converted back to a electrical signal I_{out} and V_{out} across the output impedance Z_{out} which is identical to the source impedance.

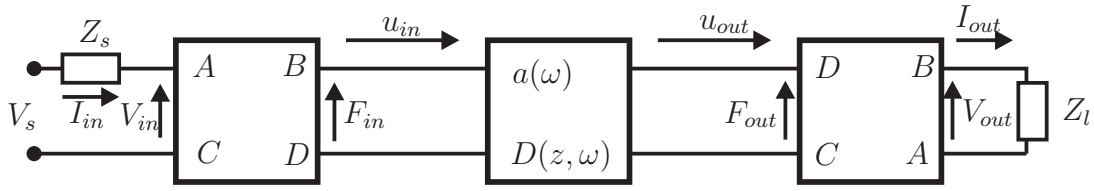

Figure 3.4: Two-Port Network Model of Calibration Measurement.

A thorough analysis of this circuit in terms of the conversion of electrical input power to acoustical input power yields the conversion efficiency from electrical to acoustic power

$$K_{EA} = \frac{|4\rho c_L a Re(Z_s)|}{|[Z_s(D-\rho c_L a C)+(B-\rho c_L a A)]^2|}, \tag{3.1}$$

where a is the area of the transducer. A similar approach for the output terms shows that the conversion efficiency from acoustic to electric power K_{AE} is identical to the expression in Equation 3.1. This means the transducer is indeed reciprocal.
With the reciprocity proven one can now use the impulse-response to obtain a transfer function. The incident acoustical energy $P_{A,inc}$ and the electrical output energy $P_{E,out}$ are connected via the conversion efficiency K

$$P_{A,inc} = \frac{P_{E,out}}{K}. \tag{3.2}$$

Using the definitions of acoustical and electrical energy one obtains an equation in terms of the incident displacement amplitude A_{inc}

$$\frac{1}{2}(\omega A_{inc})^2 \rho c_L a = \frac{\frac{1}{2}{I_{out}}^2 Re(Z_s)}{K}, \tag{3.3}$$

or

$$A_{inc} = \underbrace{\sqrt{\frac{Re(Z_s)}{\omega^2 \rho c_L a K}}}_{H} I_{out}, \tag{3.4}$$

with H being the transfer function.

Now that the transfer function is defined, a way to identify the conversion efficiency must be found. For that purpose a simple schematic of the pulse-echo setup is helpful.

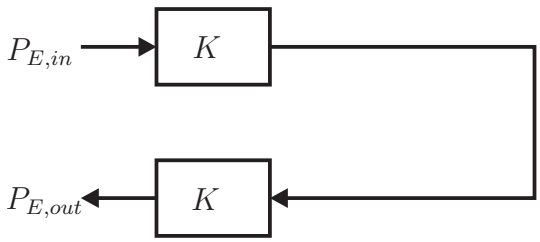

Figure 3.5: Block Diagram of Calibration Measurement.

Figure 3.5 shows the input electrical energy $P_{E,in}$ as it gets converted to acoustic energy with the efficiency K. Then the acoustic energy gets converted back to electrical energy when the signal arrives back at the transducer after reflection. Because the transducer is reciprocal, the efficiency from the acoustic energy to electrical output energy $P_{E,out}$ is K, again. Therefore one can write

$$P_{E,out} = K^2 \, P_{E,in}. \tag{3.5}$$

Substituting the energies with measurable currents and voltages yields the equation for the conversion efficiency

$$K = \frac{2 I_{out} Re\left(\frac{V_{out}}{I_{out}}\right)}{I_{in}\left(\frac{V_{out}}{I_{out}}\right) + V_{in}}. \tag{3.6}$$

Substituting Equation 3.6 into Equation 3.5 gives the expression for the transfer function

$$H = \sqrt{\frac{I_{in}\left(\frac{V_{out}}{I_{out}}\right) + V_{in}}{2\,\omega^2\,\rho\,c_L\,a\,I_{out}}}. \tag{3.7}$$

It is important to note that all variables in Equation 3.6 are defined in the frequency domain. Experimentally voltage and current are measured in the time domain. Therefore the values need to be converted into the frequency domain via the Fourier Transform. Besides that the equation shows that the transfer function can be easily obtained after measuring current and voltage at the input and the output.

3.6.2 Experimental Procedure

The first step for the calibration measurement is to clamp the specimen into the fixture. The specimen must be clamped tight enough to ensure that attaching the transmitter later on will not change the coupling situation (e.g. force on the transducers) for the receiver. On the other hand one should avoid exerting too much force on the specimen in order not to scratch the surface and not to put a significant amount of stress in the specimen. Once the sample is in the fixture, one drop of oil is applied on the receiving transducer with a syringe and the transducer is fastened to the specimen with the micrometer screw. Again one has to be careful to fasten the micrometer screw as strong as possible without damaging the sample or the transducer (especially when using transducers without backing). For multiple measurements, the position of the micrometer screw should be noted in order to reproduce the same coupling situation for all measurements. The viscosity of the oil is very low. Therefore the couplant layer changes its thickness over time. For shorter measurements this may not have a large influence but if the nonlinearity measurement extends over a longer period of time, the initial calibration might not be valid anymore. To avoid this, the transducers ideally rests at least 5 hours on the sample before the calibration is taken. The influence of the resting on the transfer function can be clearly seen in Figure 3.6. The graph shows the value of the transfer function at 10 MHz, H_2, taken over a period 26 h. In the first five hours the value of H_2 increases by $8x10^{-11}$ or 1.26 %. After that the transfer function stays constant within 0.2 %. Consequently in order

to ensure that the coupling situation at the receiver side does not change during the measurement one should wait several hours for the transducer to settle. On the other hand if time is an important issue and maximun accuracy is not absolutely required, the waiting time can be cut short because the change always stays less than 2 %.

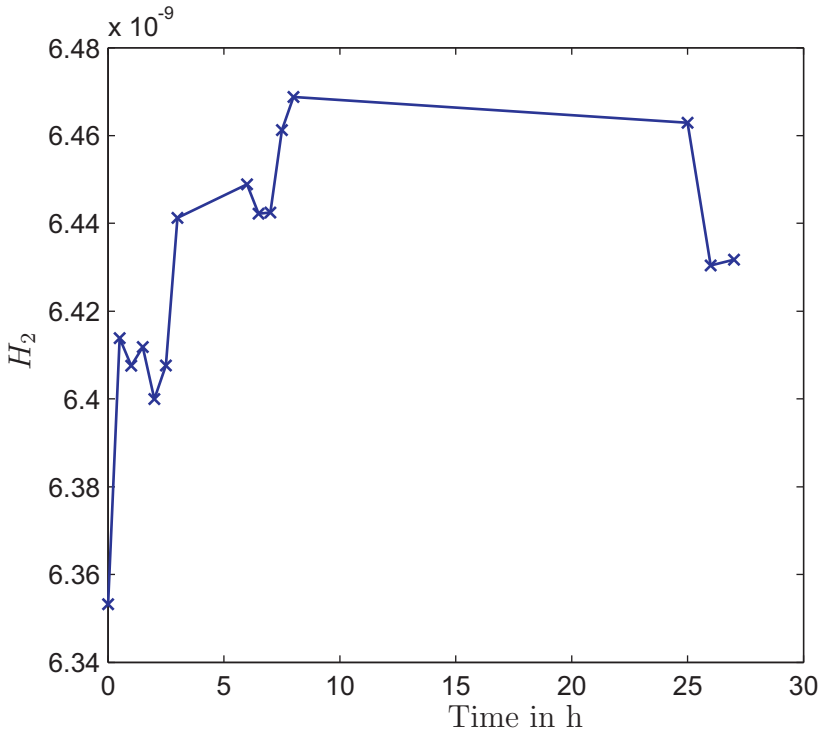

Figure 3.6: Transfer Function at 2nd Harmonic over Time.

After the transducer has settled the calibration measurement can begin. Figure 3.7 shows the basic setup of the calibration measurement. The pulser is connected to the transducer and triggers the oscilloscope. The output pulse height is set to 400 V, the input impedance to 50 Ohms and the repetition rate to 200 Hz. Voltage and current probes are connected to the cable leading to the transducer and to the oscilloscope. The oscilloscope is set to take 5000 measurements over a time period of 10 microseconds and average the measurements 512 times. These settings work for all specimens used.

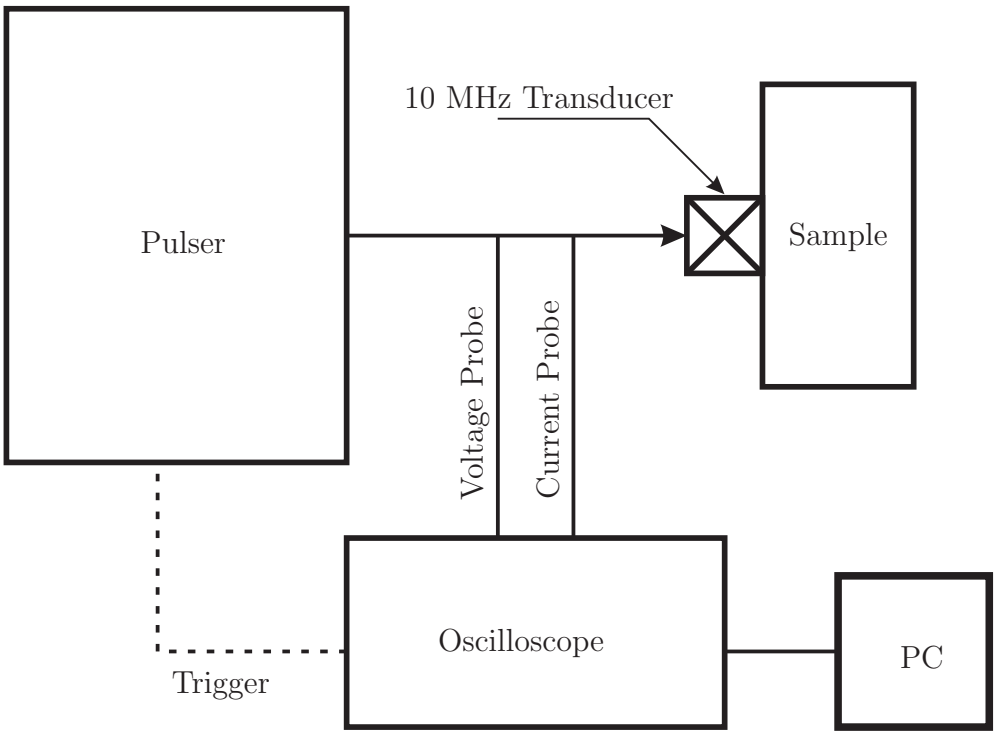

Figure 3.7: Calibration Setup.

Besides having a good resolution it is important to keep the time period long enough to capture the reflection. The initial amplitude is about 100 times larger than the reflection therefore it is important to record input impulse and reflection in two separate measurements. In the first measurement, the oscilloscope is set to fully capture the input signal in both current and voltage. In this setting, the reflection is barely visible. Therefore a second measurement is made where the sensitivity is increased to the maximum that still fully captures the reflection. The acquired records for the input and output are shown in Figures 3.8 and 3.9. This concludes the signal acquisition part of the measurement.

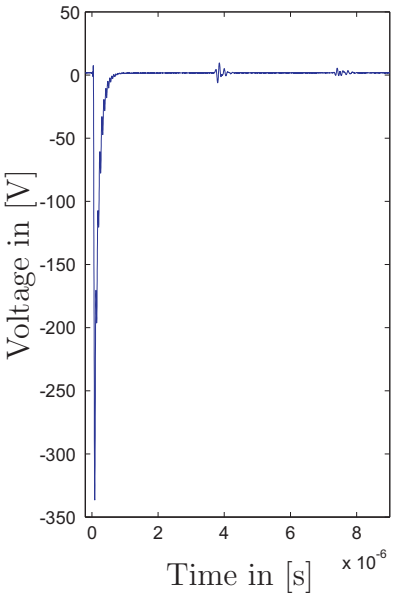

Figure 3.8: Measurement of Input Voltage.

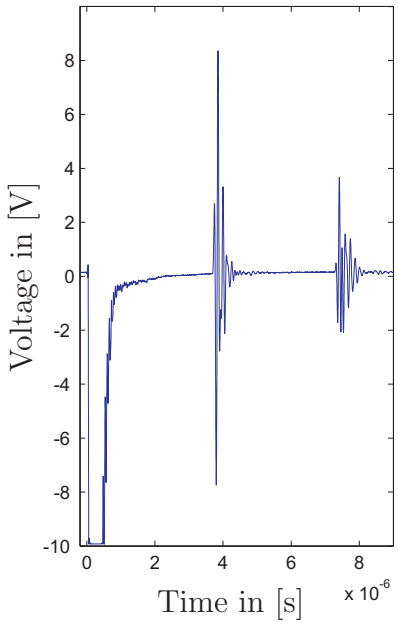

Figure 3.9: Measurement of Output Voltage

The next step is signal processing. Only a short explanation of the necessary steps is given here. More details on this topic can be found in [14]. In order to calculate the transfer function according to Equation (3.7), one needs to obtain I_{in}, V_{in}, I_{out} and V_{out} in the frequency domain. The first step to do so is windowing. The signals inherently decrease quickly. Therefore a simple rectangular window can be used without any drawbacks. It is feasible to choose all windows to have the same length and therefore avoid any corrections.

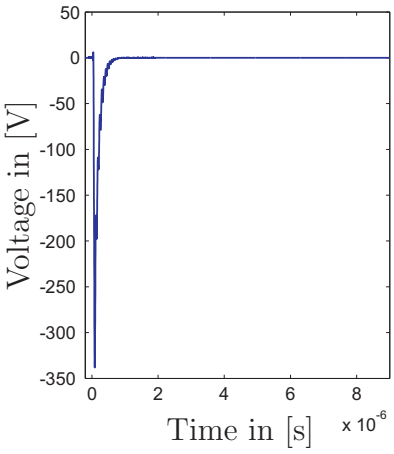

Figure 3.10: Windowed Input Signal.

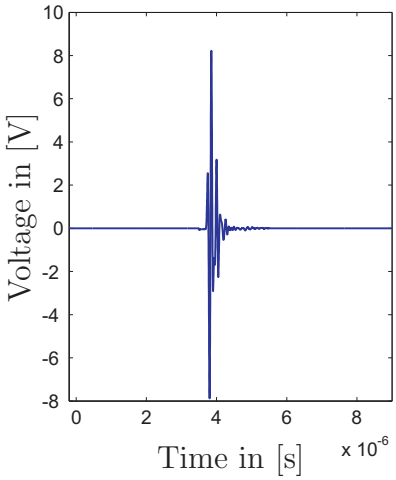

Figure 3.11: Windowed Output Signal

Figures 3.10 and 3.11 show the windowed signals. These components will then be converted to the frequency domain via the fast Fourier transform (FFT). The special form of Equation 3.7 eliminates any constant factor that is common to all parts of the signal. Therefore the length of the window does not have to be corrected for as long as all windows have the same length.

Once all components are converted one can calculate the transfer function and save the values of it at 5 MHz and 10 MHz for later use. Figure 3.12 is an typical example of the transfer function of a 10 MHz transducer. It can be seen, that the transducer is most sensitive in the frequency band from 8 to 14 MHz but still as decent sensitivity at 5 MHz. Therefore the 10 MHz transducer is a good choice as a receiver because the 5 MHz component of the signal is inherently much stronger than the 10 MHz component.

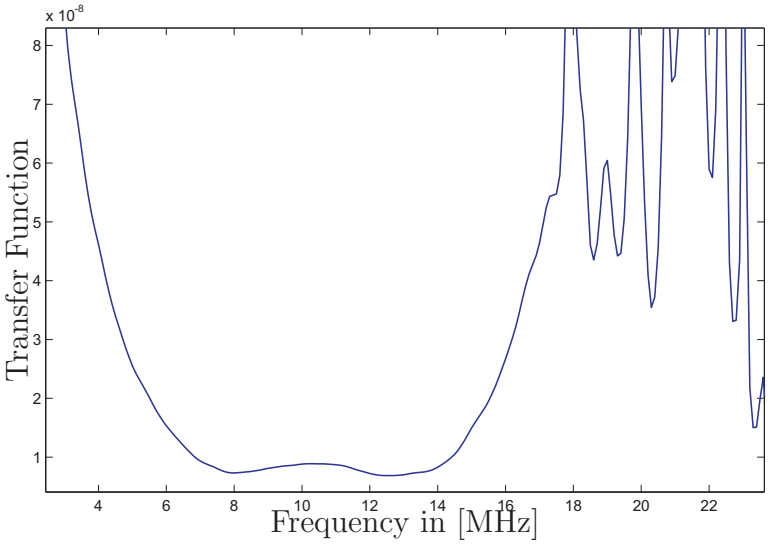

Figure 3.12: Transfer Function.

3.7 Nonlinearity Measurement Procedure

3.7.1 Theoretical Background

The principles of nonlinear wave propagation are presented in Chapter 2.3. The acoustic nonlinearity parameter is defined as

$$\beta = \frac{8A_2{c_L}^2}{\omega^2{A_1}^2x}. \tag{3.8}$$

Equation 3.8 shows that in order to obtain the nonlinearity parameter one must measure the amplitude of the fundamental and second harmonic frequencies. The following measurement is designed to do that.

3.7.2 Measurement Procedure

After the calibration is done the measurement of the nonlinearity parameter can begin. First of all the transmitter is attached in the same way the receiver has been attached. A drop of oil is applied on the surface of the transducer with a syringe. Then the transmitter is pressed against the sample via a micrometer screw and a metal pad. The measurement should be done soon after the calibration in order to maintain consistency and accuracy. Therefore it is not possible to let the transmitter

rest for 5 hours like the receiver. Still a shorter period of time, about 15 min, should be allowed for the transducer to settle and for the couplant layer to reduce its thickness. A thin couplant layer causes good transmission of ultrasonic waves through it and reduces harmonic generation from the coupling.

Before the measurement starts it is important to let the amplifier warm up. The amplifier changes its output behavior and especially its linearity with the temperature. For reasons that are explained later on, the output level will be varied to many different levels during the measurement. Therefore an absolutely steady state of the temperature cannot be achieved. To avoid high temperature gradients, it is still important to let the amplifier reach an operating temperature before the measurement starts. In order to do so the amplifier runs for 30 min at 95 % before the first measurement begins.

With the transducer attached, the experimental setup can be completed. The full arrangement can be seen in Figure 3.13. The signal from the gated amplifier gets attenuated by 6 dB and low-pass filtered before it arrives at the transmitter. After the signal passed through the sample it is received by the 10 MHz transducer and terminated in a 50 Ohm resistor matching the input impedance of the pulser. The output current is measured with the aforementioned current probe and recorded by the oscilloscope. Usually 5000 points are taken over 10 microseconds and averaged 512 times. The sensitivity is adjusted to cover the full amplitude of the signal.

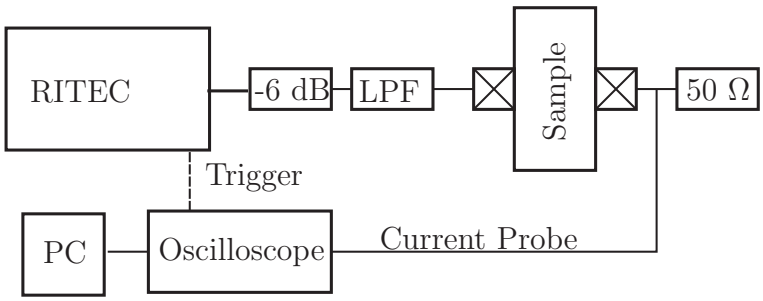

Figure 3.13: Experimental Setup for nonlinear acoustics measurements

3.7.3 Input Signal

The signal used for the ultrasonic examination is a 5 MHz toneburst. A longer signal increases the accuracy of the measurement but if the signal is too long the incident and the reflected wave interfere at the receiver side and it is impossible to extract the incident wave. Therefore the signal length is chosen to be slightly shorter than twice the thickness of the sample. This is the longest possible signal that still avoids interference at the receiver side. For example consider an aluminum sample with longitudinal wave speed $c_L = 6320$ m/s and a thickness of $h = 15$ mm. This means that the incident wave will arrive at the receiver at $t_1 = 15 \times 10^{-3}/6320\, s = 2.37\, \mu s$. The first reflection has to travel three times through the thickness and therefore will arrive at the receiver at $t_2 = 3t_1 = 7.12\, \mu s$. The maximum signal length consequently is $\Delta t = t_2 - t_1 = 4.75\, \mu s$. At a excitation frequency of $f = 5\, MHz$ this is equivalent to $n = f\, \Delta t = 23.75$ cycles. To be on the safe side and allow for some error 22 cycles would be a good choice in this case.

In order to be able to obtain the material parameter not only from single measurements but also from the slope of A_2 vs ${A_1}^2$, it is necessary to vary the output level of the amplifier. The lower starting point is either 10 % of the maximum output level if β for low drive amplitudes is of special interest or a higher value that has

to be determined experimentally that is high enough to be in the regime of a constant material nonlinearity. From the lower starting point the output level is then increased in a 5% increment until 95% is reached. Figure 3.14 shows a typical plot of β for different drive amplitudes obtained on Al2024 with a 15 cycle 5 Mhz burst with the custom transducers. As can be seen a lower starting point of 10 % reveals the typical behaviour of the β for low drive amplitudes including the characteristic Buck hook that as been observed in previous research [3]. If only the constant values of the material nonlinearity parameter is of interest, a lower starting point of 45 % can be chosen because from this output level on β is constant. Another important aspect during the measurement is to allow one minute after each 5 % increase for the amplifier to reach a constant temperature.

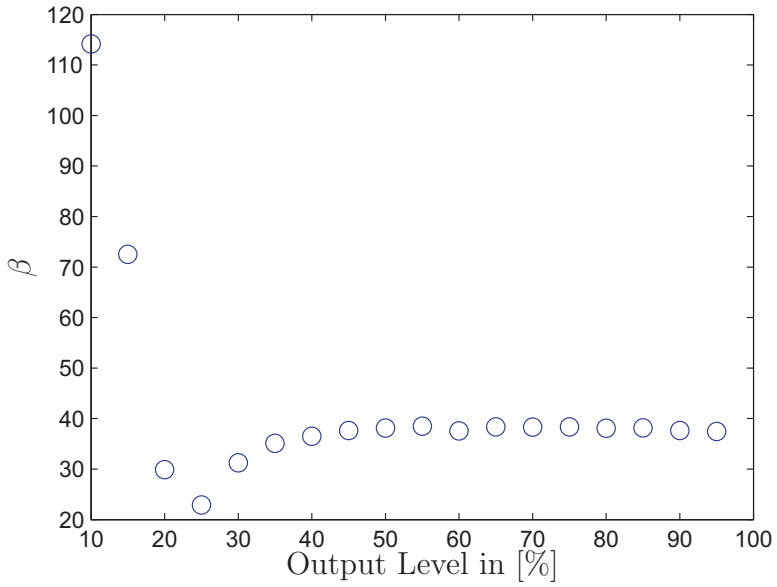

Figure 3.14: Acoustic Nonlinearity Parameter for Varying Drive Amplitude.

3.7.4 Signal Processing

After the measurement, signals in the time domain for each output level are available. The signal processing extracts the amplitudes of the first and second harmonics from this set of data and then calculates the nonlinearity. The first step of this process is

to choose a range that includes only the steady state part of the incident wave from the whole signal because the theory on which this experiment is based is only valid for steady state time harmonic signals. The selected range is chosen in such a way that it contains an integer number of cycles and has a zero crossing at the beginning and the end of it. The recorded signal and the selected range are shown in Figure 3.15. It is important to note that at this point no decision about the shape of the window or any further steps have been made. Merely the part of the signal that will be processed is selected in this step.

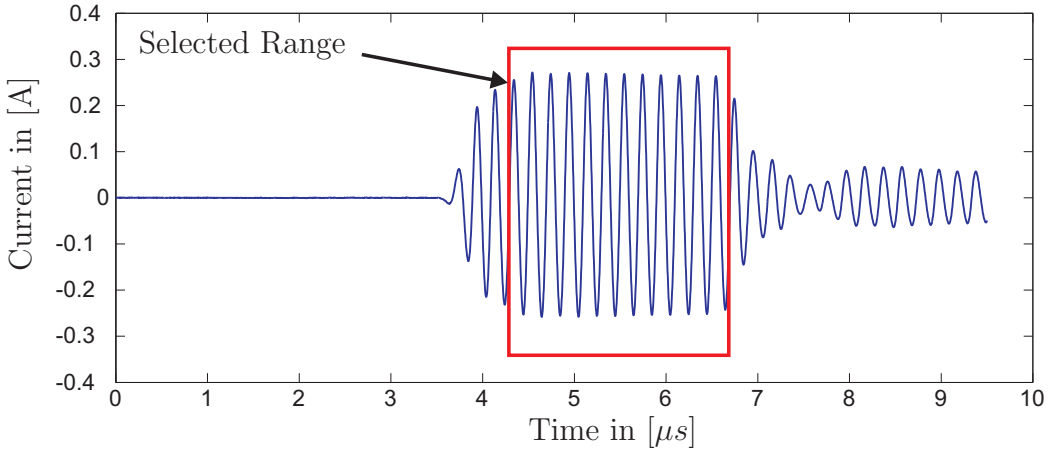

Figure 3.15: Signal from Nonlinear Measurement.

The choice of the used window often has a large influence on the accuracy of the obtained results of the frequency spectrum. Two different windows are commonly used for signal processing of nonlinear measurement data. The most common one is the Hanning window. It has relative sidelobes of -31 dB and due to its shape it gives less weight to the edges and is therefore smoothing them. The disadvantage of the window is possible spectral leakage which effectively means the second harmonic can get amplified. A more detailed explanation of the aspects of windowing can be found in [12]. The other option is the rectangular window.It has higher relative sidelobes of -13 dB but a more narrow main lobe. The main advantage of this window besides

being the simplest possible window is that it avoids spectral leakage. On the other hand, it is very sensitive to the influence of the edges of the signal, but in this experiment the window can be easily chosen to only include a full cycle and thus minimize the truncation noise that is caused by not cutting the signal at a zero crossing. Therefore the rectangular window will be used in this project. Figure 3.16 shows the two different windows. As one can see, the rectangular window gives the same weight to every part of the window while the Hanning window gives more weight to the center and less to the edges.

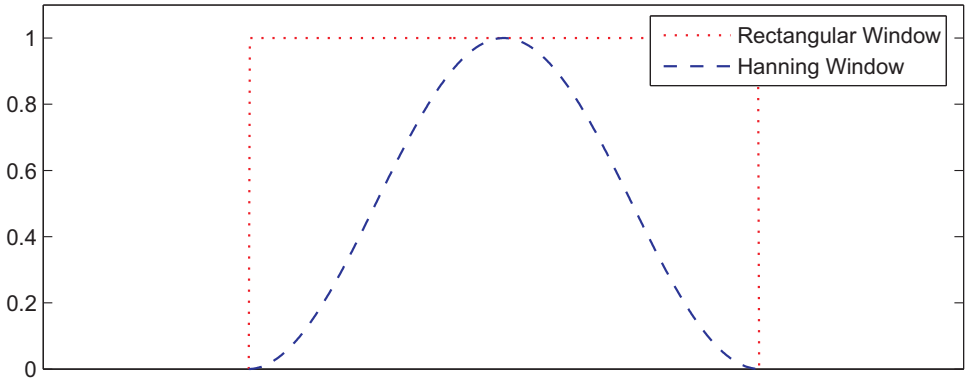

Figure 3.16: Rectangular and Hanning Window.

Comparing signal processing results of the same measurements once using the rectangular window and once using the Hanning window with zero padding as shown in Figure 3.17, one can see that both approaches yield almost the same values for high amplitudes. For lower amplitudes there is some discrepancy but that is not very important because for absolute nonlinearity calculations only high amplitudes are used.

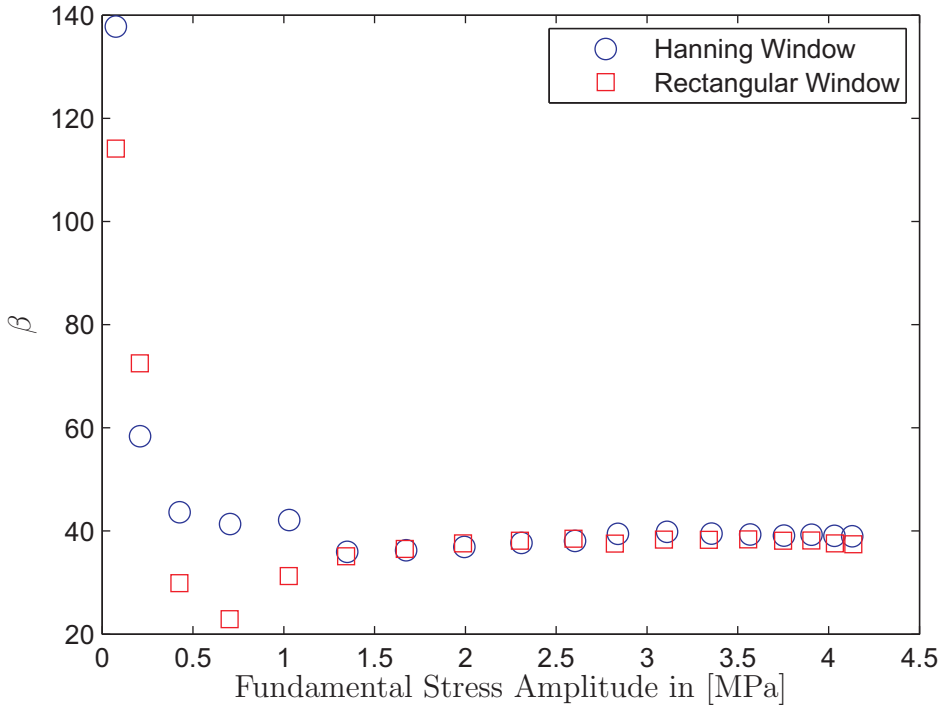

Figure 3.17: β over Stress Amplitude Calculated Using Different Windows

Usually the windowing process is combined with zero padding to obtain a finer resolution in the frequency domain by interpolation. This step is extremely important if the fundamental frequency is not a multiple integer of $\frac{f_s}{2N_s}$, where f_s is the sampling frequency and N_s is the number of samples taken. In this experiment the data is recorded at 500 Mhz with a record length of 5000 Points. This means that the fundamental frequency corresponds exactly with a discrete point after the FFT. Thus any zero padding would only smooth the curve but would not influence the result at the first and second harmonic frequencies. In order to minimize processing time and avoid other unwanted effects of zero padding, it is omitted. In summary a rectangular window without zero padding will be used. The result of the windowing with a 800 point rectangular window is shown in figure 3.18. Usually a window length that is a factor of 2 is chosen for the FFT but in this case it is more important to include an integer multiple of the wavelength into the window.

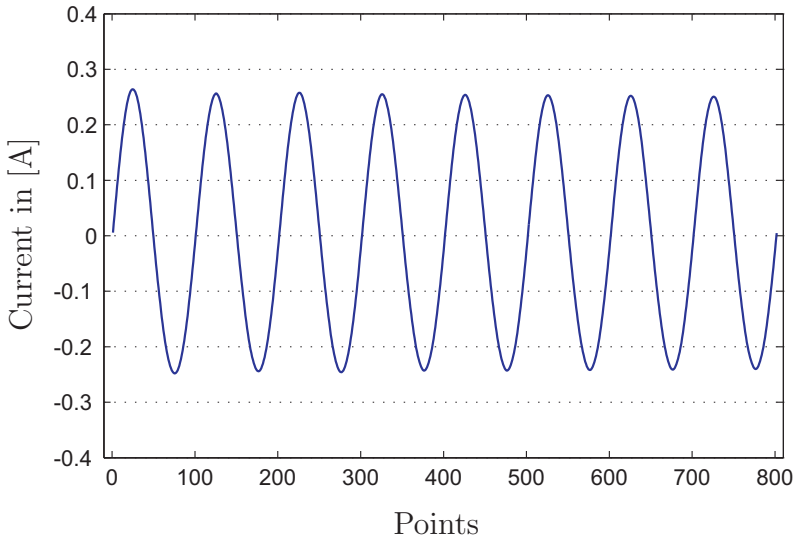

Figure 3.18: Windowed Signal.

The script integrated in MATLAB can handle FFTs on signals with any length without zero padding. For example one would use a 800 point FFT on the 800 point windowed signal in Figure 3.18. This results in a frequency spectrum that only has two clearly visible, easy to identify peaks exactly at 5 Mhz and 10 Mhz. The values that can be obtained from the frequency spectrum are still the current amplitudes and not yet related to physical displacements. To do that one simply multiplies the measured values with the transfer function obtained in the calibration measurement. The nonlinearity parameter β can theoretically be calculated from a single measurement as only A_1 and A_2 are needed. Nevertheless it increases the accuracy and repeatability if measurements at different output levels are used to obtain β. These measurements are then used to calculate a linear least square fit for A_2 vs ${A_1}^2$. From Equation 2.26 it can be seen that the slope of this graph must be $(\beta\omega^2 x)/(8{c_L}^2)$. Thus the slope of the fitted linear curve can be used to obtain the nonlinearity parameter. Figure 3.20 clearly shows that even though the experimental data does not scatter too much, single points are well off the best fit curve most likely due to the linearity of the amplifier depending on the output level.

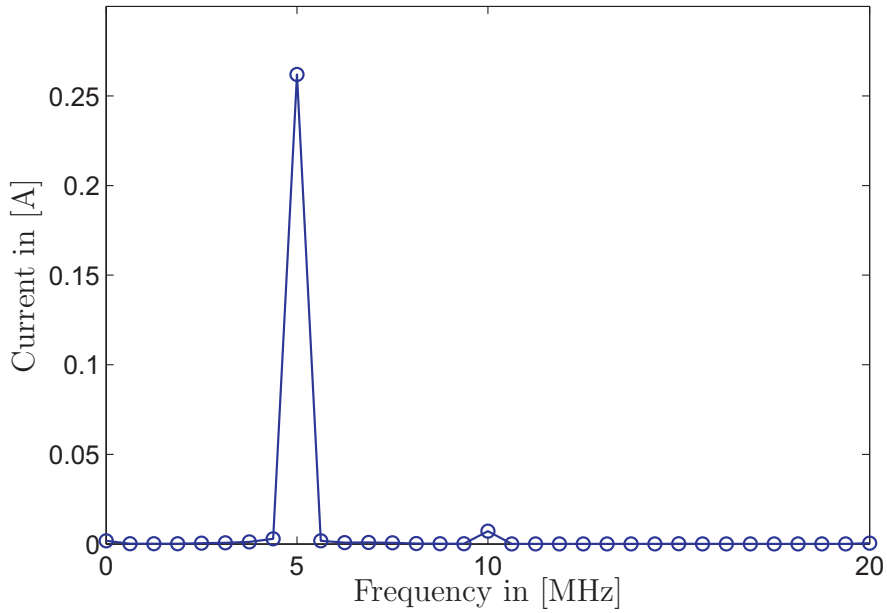

Figure 3.19: Frequency Spectrum of Signal.

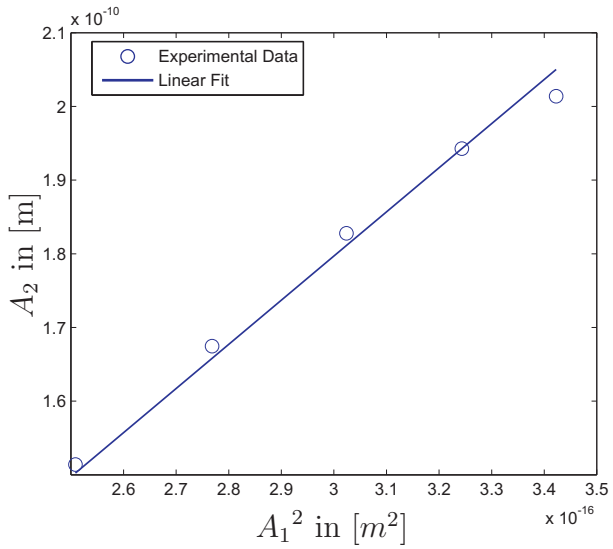

Figure 3.20: Experimental Data and Best Fit Curve of A_2 vs ${A_1}^2$.

Therefore it is important to take multiple measurements instead of just relying on a single measurement. The calculation of the best fit and the nonlinearity parameter concludes the signal processing and the whole measurement.

3.8 Specimen

There are two different kinds of specimens for this research. The first kind of specimen are undamaged samples of different materials. They are used to investigate the capabilities of the experimental setup in terms of measuring the absolute nonlinearity parameter correctly for different materials. Furthermore those specimen are used to compare different setups and to examine the repeatability of the experiment.
The second kind of specimen are samples with creep damage.

3.8.1 Undamaged Specimen

Three different materials were used to determine how accurate the experiment is: Al2024, Al7075 and fused silica. Both aluminum samples are identical in size. Figure 3.21 shows the AL7075 specimen and its dimensions. The most important number is the thickness of 19 mm because the measurements are done through the thickness of the sample. The width is 25.5 mm and the length 202 mm.

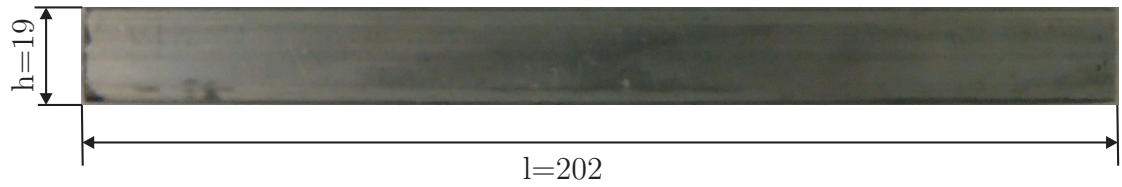

Figure 3.21: AL7075 Specimen - side view.

The surface condition of both aluminum samples is either polished by hand or by machine. The specimen are polished after several measurements, when the surface showed multiple scratches. A more detailed description of the surface condition for each measurement is given in the results section.

Material nonlinearity parameters can be calculated from material properties. Therefore there are theoretical values for the material nonlinearity for all materials. For Al2024 the theoretical value is 4.09, for Al7075 it is 7.6.

Additional measurements are done on a flat Nickel superalloy IN 100 cylinder with 25.4 mm in diameter in 12.7 thickness. Experiments to investigate the influence of welding on the nonlinearity parameter are conducted on an A36 steel strip with 6.35 mm thickness. As a non-metallic testing material fused silica is used. It has the advantage of being much harder than aluminum. Therefore the surface does not get scratches during the measurement and constant surface conditions can be sustained without any polishing. The sample is a flat cylinder of 65.5 mm diameter and 10.7 mm height. The reference value of the material nonlinearity parameter for fused silica is 12.4 [7]

3.8.2 Creep Damaged Specimen

The investigated material is A335 P22 piping steel. A335 is a carbon steel commonly used for high temperature pipes. The specimen is cut from a pipeline that has been in use for 20 year in a power plant. Though the creep damage has not been introduced in a lab environment, after the long period of time that the pipe has been in use under high temperatures and pressure it can be assumed that some creep damage is present in the sample. As already mentioned earlier, the area around the weld is very susceptible to creep. Therefore the specimen has the weld approximately in the middle, which gives the opportunity to examine both sides of it. Figure 3.22 shows the specimen and the position of the weld. The weld was made visible by etching so that the position could be determined. The thickness of the sample is 7.2 mm.

The surface of the sample is polished with a surface grinding machine before the measurements. After the nonlinear measurements are completed, the specimen is solution annealed for 2 hours at 1100 C. This treatment reduces the dislocation

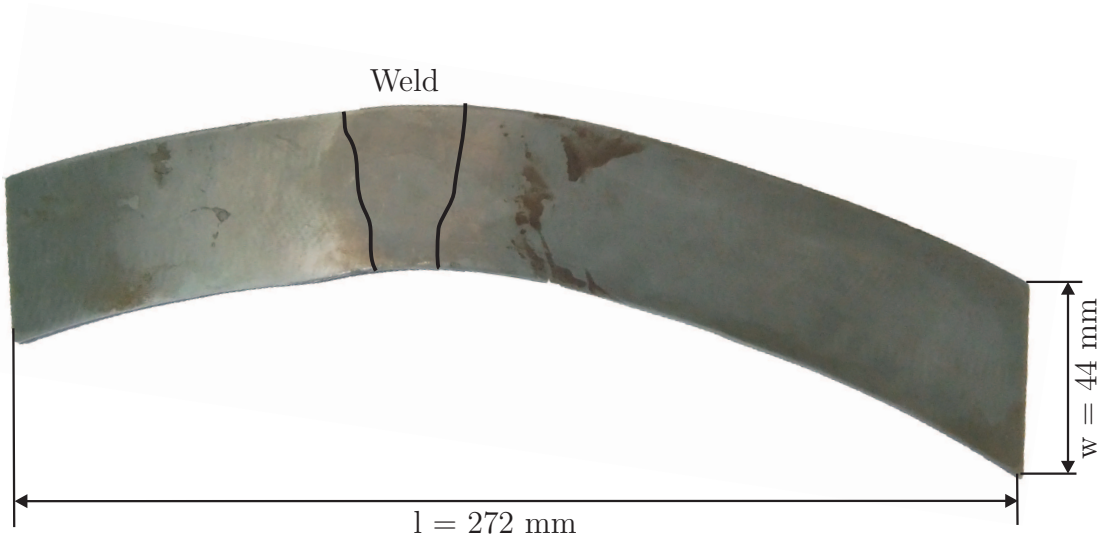

Figure 3.22: A335 P22 Steel Creep Specimen with Position of Weld.

density and annihilates voids.

It is assumed that the material comes back to a configuration comparable to its virgin state. Therefore measurements after the annealing can be used to put the initial measurements on the creep damaged specimen in context. The heat treatment caused significant corrosion of the sample. Therefore it was polished again afterwards. The same polishing procedure was used both times. Therefore the surface condition for all measurements is basically identical.

CHAPTER IV

RESULTS

4.1 Calibration

The calibration measurement is performed before every nonlinearity measurement. If it is not accurate, any information from the later measurements will be useless. Furthermore the instrumentation influence on this measurement is much smaller than on the nonlinearity measurement. Therefore it is reasonable to first make sure that the calibration measurement works reliably and delivers reasonable values.

It is difficult to judge the accuracy of the calibration because there are not many alternative possibilities to calculate the transfer function. One option would be the alternative calibration according to [16] but it is not realized within this project due to time restrictions. Still there is an option to validate the measurements; the comparison with other published calibration curves shows if the same trends are visible. A first comparison can be done between Figure 3.12 and the calibration curve in [7]. Both transfer function were obtained for fluid coupled $LiNbO_3$ transducers but even Salol bonded $LiNbO_3$ transducers give similar results. The main characteristic of the curves is the reduced sensitivity below about half the center frequency of the transducer, a minimum value of the transfer function around the magnitude of 1×10^{-8} close to the center frequency and increasingly bad sensitivity with a lot of noise above 150 % of the center frequency. In conclusion, one can say that the shape and values of the transfer function obatained in this resarch and those in [7] show very strong correlation which suggests, that the calibration measurement is correct.

Proving the repeatability of the calibration is another complicated issue. The very

nature of a calibration prohibits absolutely identical outcomes for two different measurements. However for two calibration measurements on the same surface,with the same transducers and the same couplant should result in very similar calibration curves. Figure 4.1 shows four different calibration curves, all taken on the same sample but with the transducers reattached between the measurements.

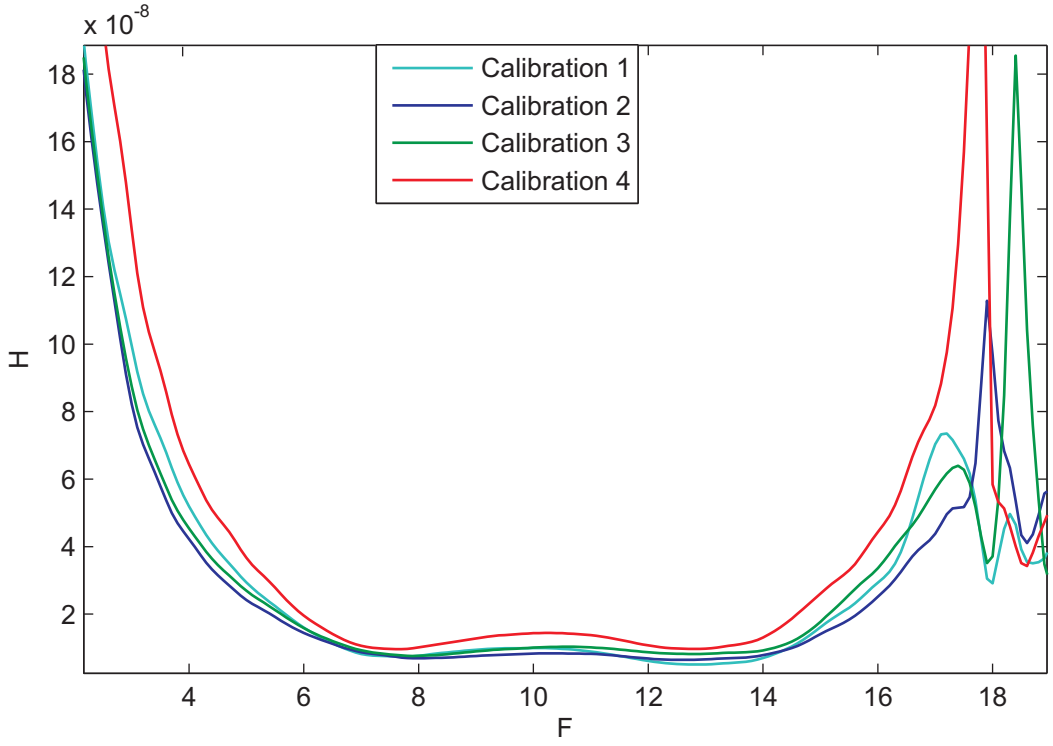

Figure 4.1: Transfer Functions Obtained by four Measurements on the Same Sample.

It is obvious that all transfer functions are very similar in terms of shape. The values however show some significant scatter. At 5 Mhz, the values of the transfer functions are between $2.42e-8$ and $2.94e-8$ which is equivalent to a difference of 21.5%. At 10 Mhz the transfer functions are between $8.28e-9$ and $1.00e-8$ which is a margin of 21%. This is a high variation, but it is plausible to assume that the coupling condition changes each time the tranducer is reattached causing the transfer function to change, too. This shows that the calibration measurement must be performed before every nonlinear measurement.

Another sanity check is performed by calculating the impedance. Since the input impedance is known to be 50 Ohms and can also be calculated from the reflected signal, one can compare those two values. A significant discrepancy is a strong hint towards a wrong setup.

4.2 Nonlinear Measurement

4.2.1 Performance of Different Transducers

The transducers are one of the most important parts of the setup. If they do not convert electrical signals to acoustic signals precisely, obtaining good results is impossible. The starting point for the transducers are the standard $LiNbO_3$ transducers. In an effort to reduce sources of nonlinearity, those transducers have been compared to $LiNbO_3$ crystal transducers and custom made cased $LiNbO_3$ transducers without backing.

In order to compare the standard transducers to the crystals, measurements on an AL2024 sample are taken once with fluid coupled standard transducers as transmitter and receiver and once with Salol bonded crystal as transmitter and fluid coupled standard transducer as receiver. With this setup only the transmitting transducers can be compared but it already gives an idea about how much the casing and backing of the standard transducer change the signal. A comparison with a setup only with crystals is not possible due to the lack of a working 10 MHz crystal transducer. Figure 4.2 shows the signals from crystal and standard transducer for comparison. The crystal produces a much stronger signal which means that the casing and backing of the standard transducer reduce the efficiency of it largely. Part of the reason for the drastic difference is the different bonding. But experiments with fluid coupled crystals show similar results therefore proving that the crystal transducer really is much more efficient than the standard transducer. More important than the strength of the signal is how clean it is.

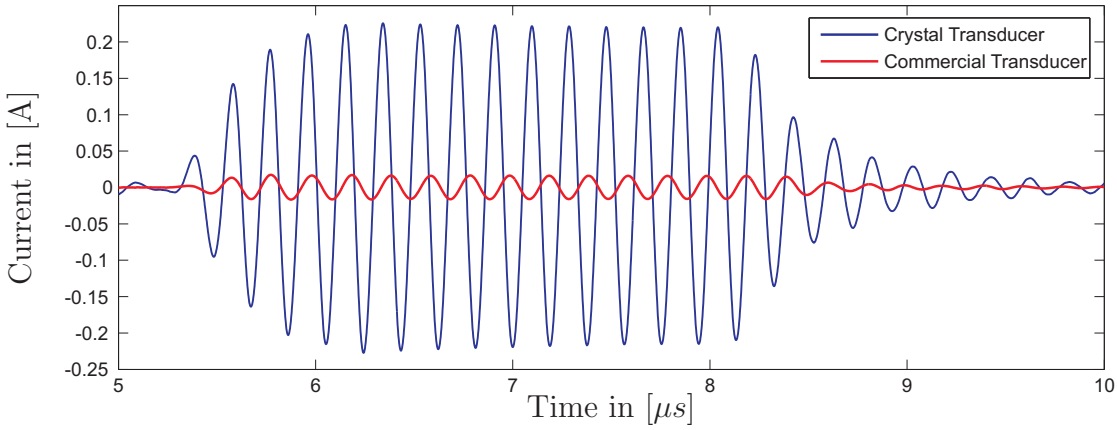

Figure 4.2: Signals from Crystal and standard Transducer

Comparing nonlinearity parameters on Al2024 with the rest of the setup being the same for both transducer configurations shows that the crystal ($\beta = 10.18$) is also much more linear than the standard transducer ($\beta = 19.23$). Even though the crystal delivers higher outputs and more linearity, the standard transducer is still the better choice to make many measurements because it is much easier to handle. The crystals are very fragile and bonding is very time consuming.

With the crystal transducer being better in the output behavior and the standard transducers being better in handling a combination of both seems to be the ideal transducer. In order to maintain the easy handling, the case of the transducer must be kept on . This case protects the crystal and facilitates quick fluid coupling. The backing on the other hand only reduces ringing slightly and makes the transducer more durable. At the same time it damps the crystal vibration which reduces its efficiency and might cause nonlinearity. Therefore the first step is to get transducers that are easy to handle and have a better output behavior than the standard transducers is to get encased crystal transducers without backing. Valpey Fisher made those transducers specifically for this research project. A comparison of their performance is done on Al7075. As Figure 4.3 shows, the nonlinearity parameter is lower with the standard transducers. This could mean that the custom transducer is in fact

less linear than the custom transducer. Another option that has not been examined so far is the relative phase angle. If the phase shift of the transducers is different, it is impossible to infer the linearity of the transducers just from the measured nonlinearity parameter because constructive and destructive interference can occur. For now it can only be observed that the nonlinearity parameters measured with the custom transducers are generally higher. Yet the custom transducers have some advantages. In the plot of the nonlinearity parameter from the custom transducer the characteristic Buck hook [3] can be observed which indicates a high sensitivity. Furthermore the output signal is up to 47 % higher with the custom transducers. They also show more ringing than the standard transducer but that does not affect the measurement. In conlusion it is not possible to predict which transducers will give better results. More measurements will show which transducer performs better.

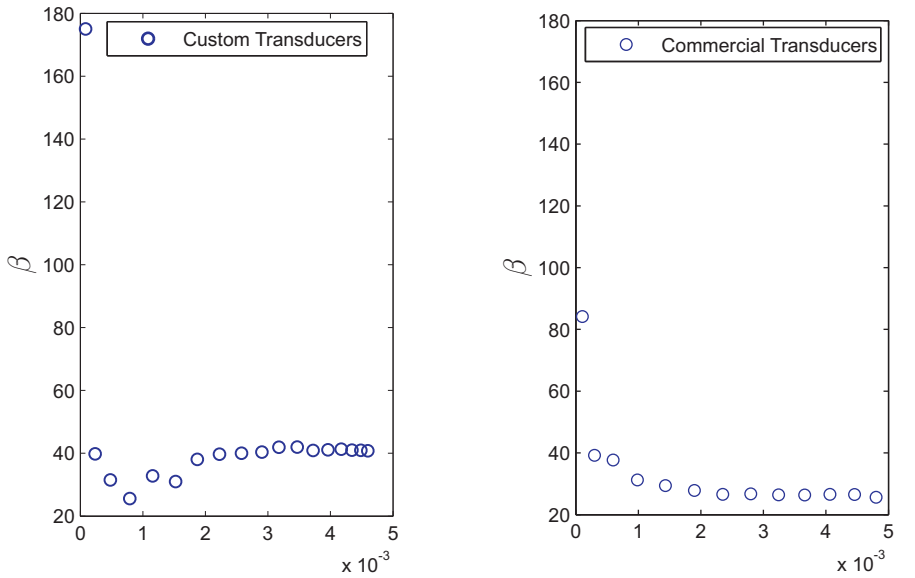

Figure 4.3: Material Nonlinearity Measured with Custom and standard Transducers

4.2.2 Improvements on Initial Setup

During this research many different setups have been tested in an effort to improve the performance. The setup found to deliver the best results is presented in the Experimental Setup chapter. This section shows how different setups affect the results. The initial setup shown in Figure 4.4 is based on [7].

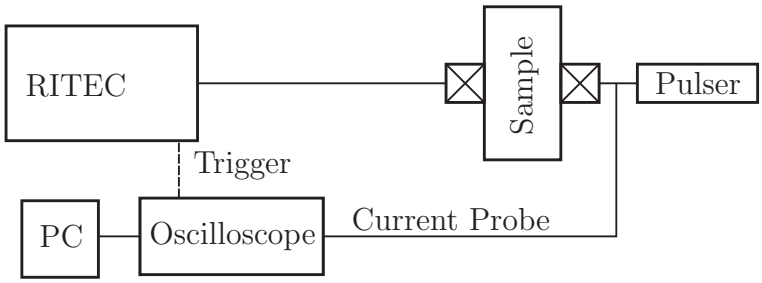

Figure 4.4: Initial Setup for Nonlinear Measurements.

The main difference of the setup compared to the one presented earlier, is that the signal does not get low-pass filtered or attenuated before it gets to the transmitter and instead of a 50 Ohm resistance as termination, the 50 Ohm input impedance of the pulser is used. Of course the pulser is switched off during the nonlinearity measurement and only acts as passive load.

This setup is not useful for nonlinear measurements because the nonlinearity introduced by the instrumentation overwhelms the material nonlinearity by far. For example absolute nonlinearity measurements on Al2024 with this setup yield $\beta = 122.29$, compared to a theoretical value of $\beta = 4.09$. The first step to improve the performance is to replace the pulser with a 50 Ohm resistance. This already reduces the extraneous nonlinearity greatly. The exact construction of the pulser is not known therefore determining the source of the distortion is not possible. But comparing signals with pulser and 50 Ohm resistance as termination identifies the pulser clearly as a source of nonlinearity. For the comparison two measurements on Al2024 are taken.

The used signal for both is a 15 cycle, 5 MHz toneburst at 95 % output level of the amplifier. The first setup is identical to the one shown in Figure 4.4. For the second measurement the pulser is replaced by a 50 Ohm resistance. The result is shown in Figure 4.5.

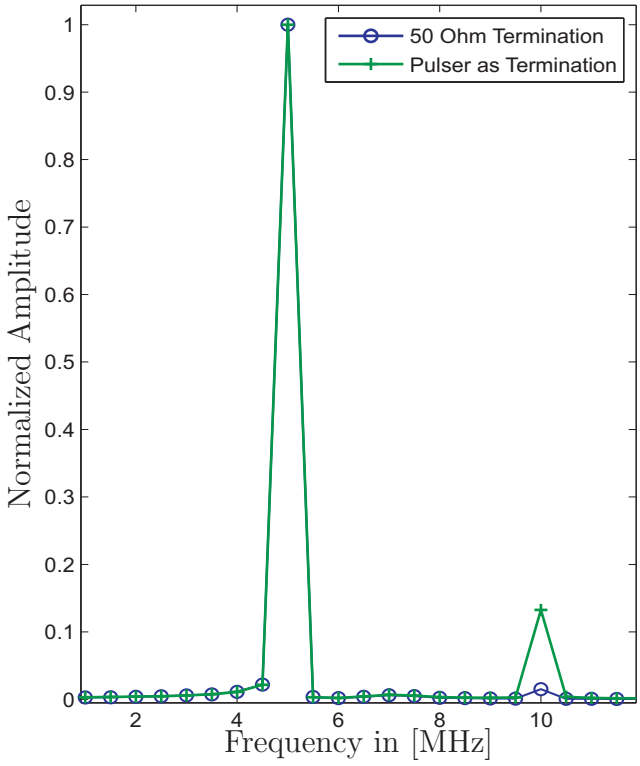

Figure 4.5: FFT of Signals from Nonlinearity Measurement with Different Terminations.

It can be clearly seen that the second harmonic is much smaller with the passive 50 Ohm termination than with the pulser. In fact the active elements in the pulser generated most of the nonlinearity. The nonlinearity factor gets reduced to $\beta = 14.65$ under the same conditions.

To further decrease the nonlinearity introduced by the instrumentation a low-pass

filter and an attenuator are installed between the amplifier and the transmitter. The low-pass filter eliminates high frequency components in the signal from the amplifier while the attenuator provides a constant impedance to the filter which increases the filter performance. The improvement of the signal by using this setup has already been pointed out in Chapter 3.

4.2.3 Nonlinearity Parameter of Different Materials

In general it can be said that no measurement resulted in values close to the theoretical values given in Chapter 2. The reason for that can be various and will be discussed later in this thesis. However measurements of different materials can be used to evaluate whether the measurements are at least related to the material nonlinearity. For that purpose nonlinearity measurements on three different materials, Al2024, Al7075 and fused silica are done. The setup used for this measurements is equivalent to the one presented in the Experimental Setup Chapter besides the omission of the attenuator. For all measurement the custom transducers are used. The input signal is a 5 MHz toneburst of 15 cycles for Al2024 and Al7075 and a 12 cycle burst for the fused silica sample. All samples are polished prior to the measurements. The results of the experiment are summarized in Table 4.1. The given reference values for Al2024 and Al7075 samples are the theoretical values. For fused silica the reference value is taken from [7]. It is obvious that the experimental results are far too high compared

Table 4.1: Experimental Material Nonlinearity Parameter for Different Materials

Material	Experimental Result	Reference Value
Al2024	43.01	4.09
Al7075	50.61	7.6
Fused Silica	68.42	12.4

to the reference values. But the measurements put the material in the right order in

terms of their nonlinearity. This means that relative measurements of nonlinearity are possible with the presented experimental setup. Moreover other measurements on the same materials have yielded values that are closer to the reference. Those measurements have been taken with different setups, corrupting the comparability. Therefore these experiments with consistent experimental setup are necessary.

4.2.4 Repeatability

Due to time restrictions, most measurements in this project have not been repeated a sufficient number of times for the calculation of error bars or other statistical examinations. However a set of experiments are conducted to investigate the repeatability of the measurements. For this experiment measurements on the same material are taken four times in a row. Between the measurements the transducers are removed, the sample is cleaned, and then the transducers are reattached. That way each time a new bonding situation is created. The repeatability test is done on Al2024, Al7075 and IN100 samples in order to examine influences of the material on the repeatability. The results of this test can be seen in Table 4.2. It shows β_1 to β_4, the results of the nonlinearity measurement, together with the mean and standard deviation of the measurements for all three materials. In can be clearly seen that the standard deviation for Al2024 is relatively much higher than the standard deviation of the other two materials. It is reasonable to assume that measurements on materials with lower nonlinearity have more scatter because extraneous nonlinearity that can cause variations relatively accounts for a larger percentage of the total nonlinearity. With that

Table 4.2: Results of Repeatability Test on Different Materials.

Material	β_1	β_2	β_3	β_4	**Mean**	**Deviation**
AL 2024	14.26	10.71	11.28	14.97	**12.8**	**2.12**
Al 7075	28.86	25.19	28.21	27.89	**27.54**	**1.62**
IN 100	69.94	64.40	72.98	66.94	**68.57**	**3.71**

in mind the repeatability test leads to two conclusions. First of all there is significant scatter at least for materials with low material nonlinearity. Secondly, considering the magnitude of the change in nonlinearity caused by creep damage as for example presented in [19], even with a deviation of 16% (for measurments on Al2024) one should be able to track creep damage with this technique.

4.2.5 Influence of the Surface Condition

In all results presented so far, remarks about the surface condition can be found. The reason for that is a very strong influence of the surface condition on the measurement. The rougher the surface, the more fluid will be in the layer between transducer and sample. This introduces a large source of nonlinearity. Furthermore polishing the surface, especially by hand can result in the two surfaces of the specimen not being parallel anymore. The exact condition of the surface is hard to quantify but the influence of different surface conditions can easily be seen. Three measurements on an Al2024 specimen employing the same setup (equivalent to the on presented in the Experimental Setup Chapter minus LPF and attenuator), standard transducers and signals (15 cycle 5 MHz toneburst) can be used to show the influence of the surface. The first measurement is done after hand-polishing the sample up to a 1200 grit resulting in $\beta = 12.12$. For the second measurement the specimen has been hand-polished again with a 1200 grit resulting in $\beta = 20.5$. The third measurement is done after machine-polishing the sample up to a 1000 grit resulting in $\beta = 10.46$. Though the sample was always polished the results vary by factor 2. The reason for the very high value of the second measurement might be that the surfaces have not been parallel anymore due to some uneven hand polishing. The strong variations suggest that one should use a machine to polish the sample because that promises the most repeatable surface conditions.

4.2.6 Evaluation of the Signal Processing

Considering the performance of the measurements each step that leads to the results has to be questioned. A crucial part on the way to the final result is the signal processing. Therefore it has to be made sure that it is accurate. The most important aspect of the signal processing is the correct representation of the frequency components. For the fundamental amplitude there is a very simple way to verify the value. All signals recorded in this research are dominated by the fundamental frequency. The amplitude of the second harmonic is around 100 times smaller than the fundamental amplitude. Thus it is a good approximation to assume that the fundamental amplitude should be equivalent to the amplitude of the recorded signal. The validation of the second harmonic is more complicated. In order to obtain the second harmonic amplitude that can be compared to the result of the FFT, one has to use a high pass filter to extract the second harmonic component of the output-signal. Comparing the filtered output signal and the result of the signal processing one has to keep in mind that the filter has some loss which means the filtered signal is expected to be slightly lower than the second harmonic amplitude obtained by the signal processing.

In order to make the comparisons just described, a 30 cycle, 5 MHz, 95% output level signal is recorded once without filter and once with filter. The amplitude of the unfiltered signal is then compared to the first harmonic amplitude and the amplitude of the filtered signal is compared to the second harmonic amplitude. Figure 4.6 shows the frequency spectrum of the unfiltered signal with the filtered and un-filtered time-domain signals. The peak at 5 MHz in the frequency spectrum has the value 15.13. The average amplitude in the window used to obtain the FFT is 15.16. This shows a very good correlation to the value in the FFT. The value of the frequency spectrum at the second harmonic is 0.63. The peaks of the filtered signal are between 0.56 and 0.49. As expected the filtered signal is slightly lower than the value in the FFT.

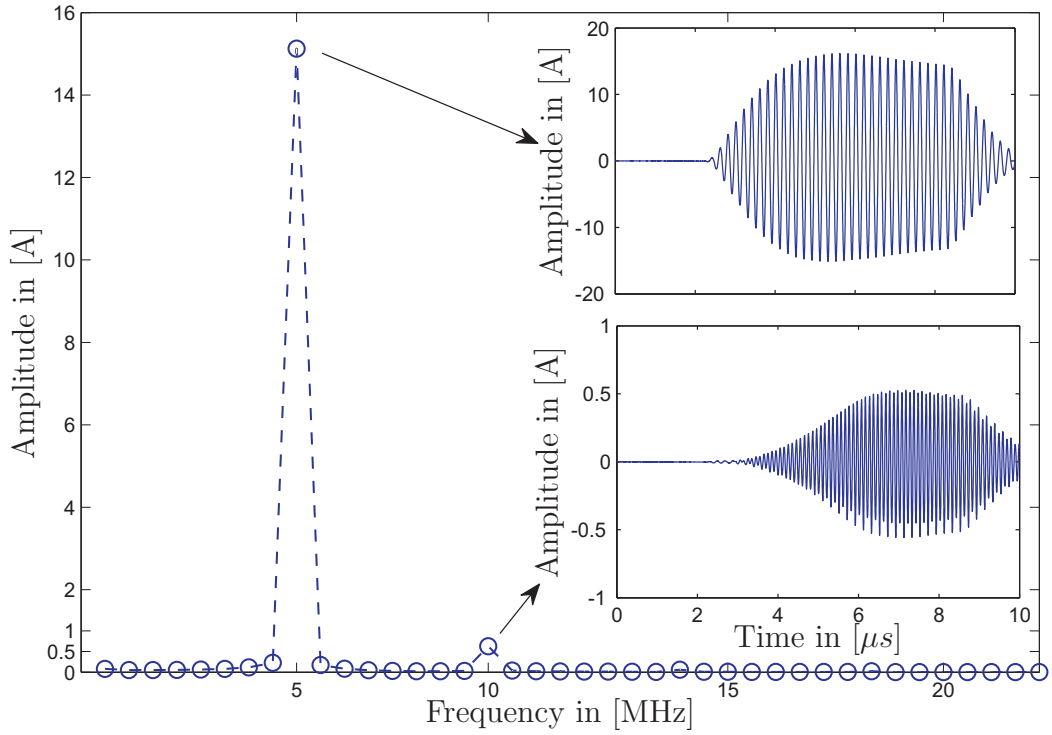

Figure 4.6: FFT and Corresponding Time-Domain Signals

Overall in can be concluded that the values obtained from the signal processing are a correct representation of the frequency components.

4.3 Creep Damage Detection

4.3.1 Nonlinearity Measurement on the as-received Creep Damaged Specimen

Knowing about the capabilities and limitations of the technique, one can now move on and use it to detect creep damage. To do so measurements on the creep damaged specimen described in Section 3.8.2 are taken. A series of measurements mostly along the middle line of the curve plate specimen are taken. For the measurements, the exact setup presented in Chapter 3 is used both with standard and custom transducers. The test signal is always a 11 cycle 5 MHz toneburst. The output level of the amplifier is varied from 40 % to 95 %.

The first set of measurements is done along the middle line using standard transducers.

As the HAZ is most susceptible to creep, an increase in nonlinearity in that area is expected. The weld has many impurities (so it has different material properties) which means the nonlinearity can hardly be compared to the rest of the material. In order to measure the nonlinearity around the weld, the nonlinearity parameter at the points marked in Figure 4.7 is taken. It is important to note that the fixture used is not designed to facilitate measurements at exactly specified positions. Therefore positioning the transducers is very complicated and it is not possible to measure the exact same point twice.

Figure 4.7: Position of Examined Points on the Specimen for the First Set of Measurements.

The measurements result in the following map of material nonlinearity. The first thing to notice is the very large nonlinearity at Point 8. This does not actually represent a real increase compared to the neighboring points but a false measurement. A look at the recorded signals reveals that the output strength at this point is factor 3 smaller than for all other points. This indicates very bad coupling caused probably by the transducer clamped against the sample at an angle and therefore not in full contact. Thus this point should be ignored for the interpretation of the measurement.

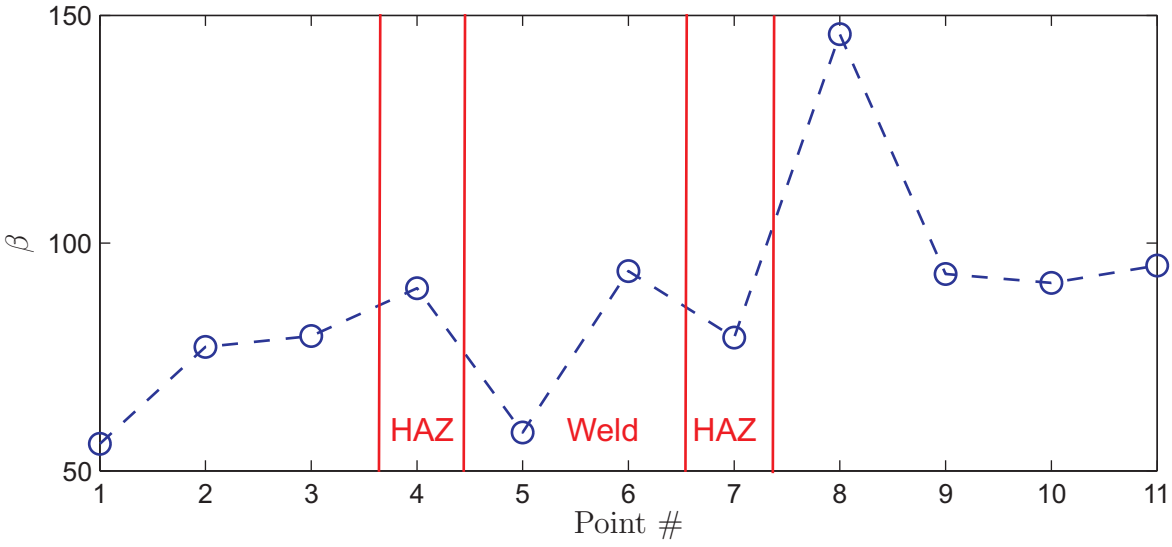

Figure 4.8: Material Nonlinearity at the Points showed in Figure 4.7.

This results in the graph shown in Figure 4.9. It can be seen that as expected the nonlinearity increases from Point 1 in the base material to Point 4 in the HAZ. Point 5 and Point 6, both in the weld, show very different nonlinearities which is most likely connected to impurities in the weld. Points 7 to 11 have roughly constant material nonlinearity which contradicts the idea that the highest level of nonlinearity should be found in the HAZ.

Another set of measurements is taken to validate the first measurement and more precisely examine the area around the weld. This time the custom transducers are used. The examined points are marked in Figure 4.10. This again results in a map of material nonlinearity. The initial measurement only included points 1 - 13. The previous measurement showed a high nonlinearity at Point 5. The fist measurement at Point 5 in this set of measurements does not show an increase in nonlinearity compared to the neighboring points. In order to examine the area more closely the additional Points a and b have been taken. The results of points 1 - 13 can be seen in Figure 4.11.

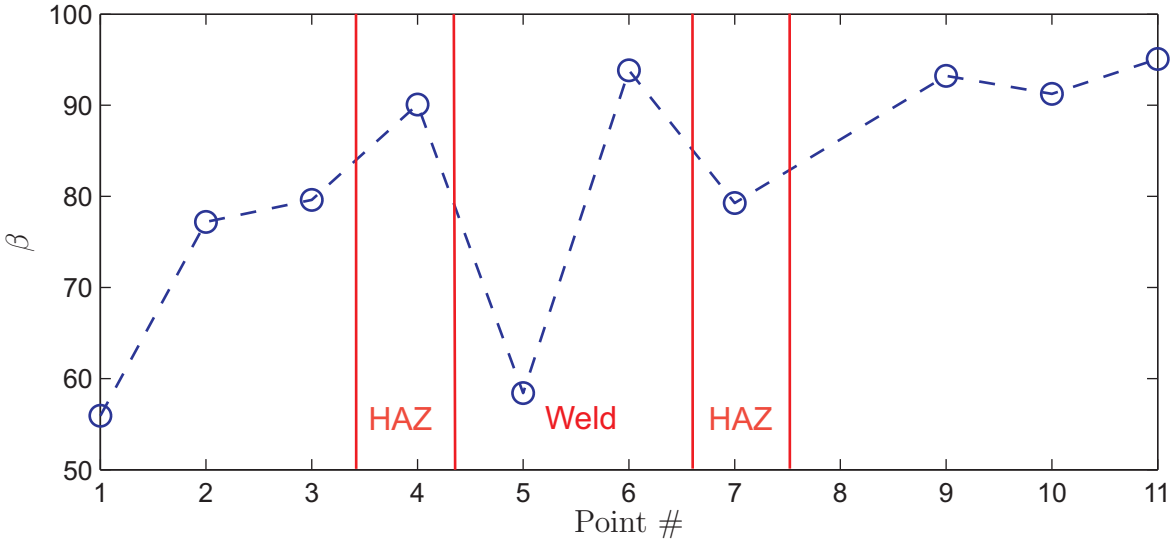

Figure 4.9: Material Nonlinearity at the Points showed in Figure 4.7 without Point 8.

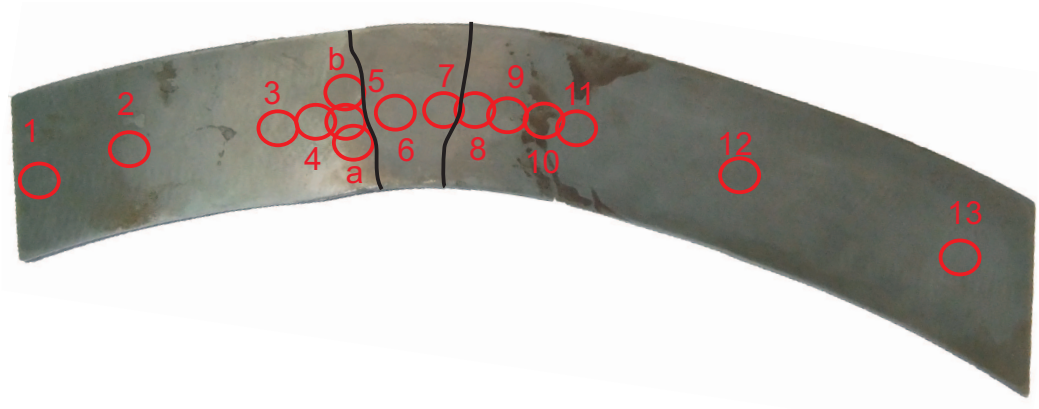

Figure 4.10: Position of Examined Points on the Specimen for the Second Set of Measurements.

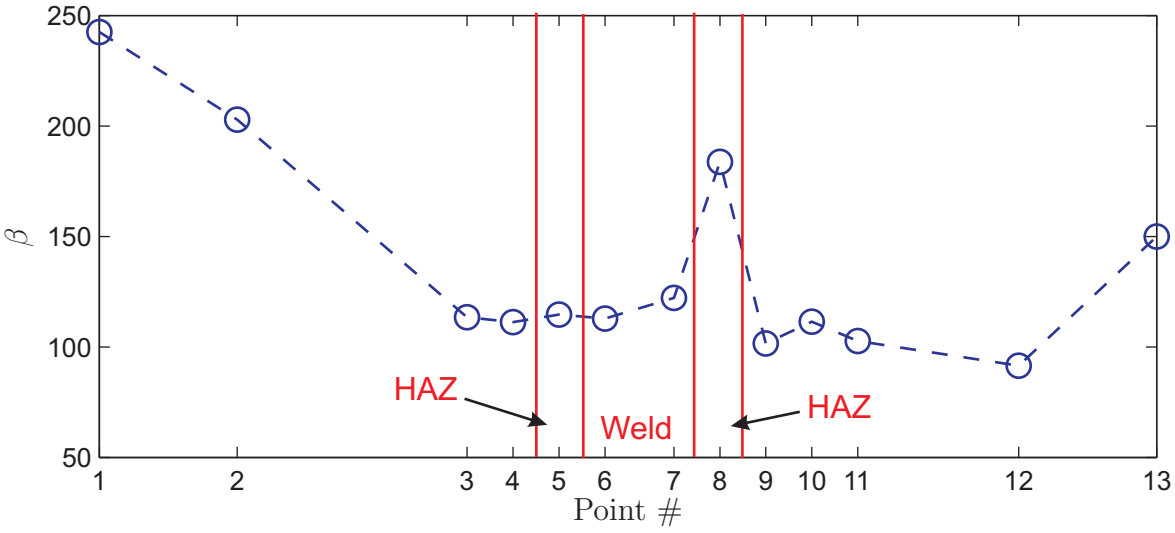

Figure 4.11: Material Nonlinearity at the Points 1 - 13 of the Second Set of Measurements.

A very high nonlinearity can be observed towards the edges of the specimen. This could be caused by the specimen not being absolutely even but it is not further investigated because the focus of this research is on the damage in and around the HAZ. Focusing on the area around the weld and including Point a and b into the graph yields Figure 4.12. It can be seen that while the points 7 - 12 on the right side of the weld show the expected behavior: A very high nonlinearity at Point 8 in the HAZ and decreasing nonlinearity for the points further away from the weld, the points 3 - 6 show very constant nonlinearity parameters even though the Points are in the base material, the HAZ, and the weld respectively. Measurements a and b however prove that the HAZ has indeed an elevated level of nonlinearity, at least at certain points. It is difficult to infer the reason for the localization without looking closely at the microstructure. Any anomaly of the microstructure from an increase in void or dislocation density to micro cracks could cause an increase in material nonlinearity. In order to get a better sense of how much the nonlinearity increases in the weld, the Points 5, a, and b are replaced by a single Point representing the average value of the three points. This results in the graph of Figure 4.13.

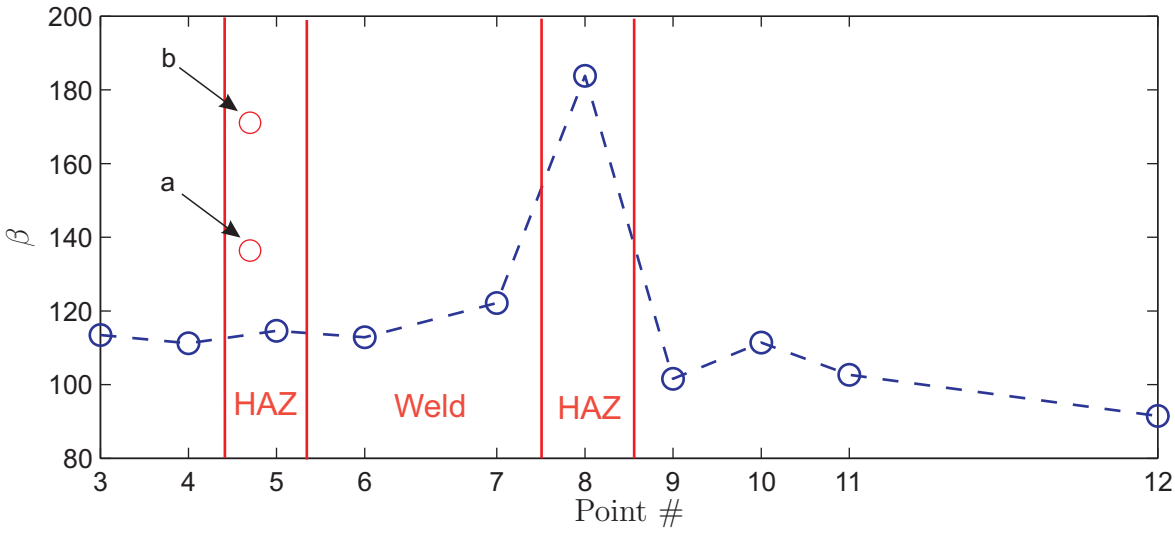

Figure 4.12: Material Nonlinearity at the Points 3 - 12 as well as Points a and b of the Second Set of Measurements.

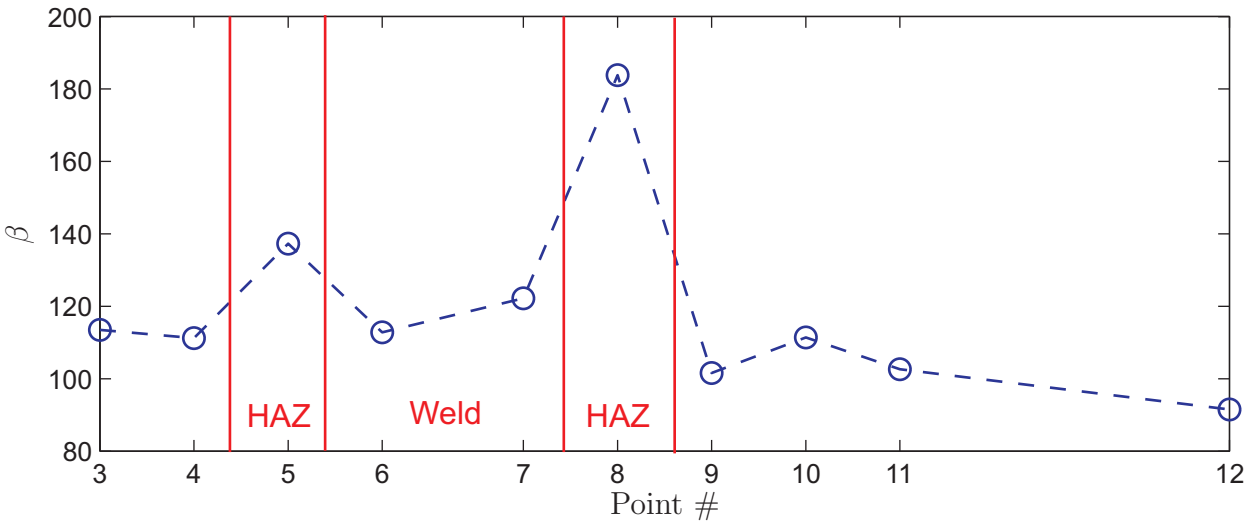

Figure 4.13: Material Nonlinearity at the Points 3 - 12; Points 5, a, and b are replaced by a single Point representing their average.

It is important to note that this time the signal strength of the measurement at Point 8 is on the same level as the other measurements, suggesting it is a valid measurement.

A third measurement is done with the custom transducers to verify the results but after two points the signal strength decreased significantly.

Figure 4.14 shows the two signals of the custom transducer at 95 % output level. The red curve is from the second set of measurement, the blue curve is taken during the attempt of the third set of measurements. The differeence between the two curves is so large that the results of the measurements cannot be compared. The reason for the decrease in signal strength is most likely that at one of the transducers the crystal was pushed into the casing. This can happen with the custom transducers because they do no have backing.

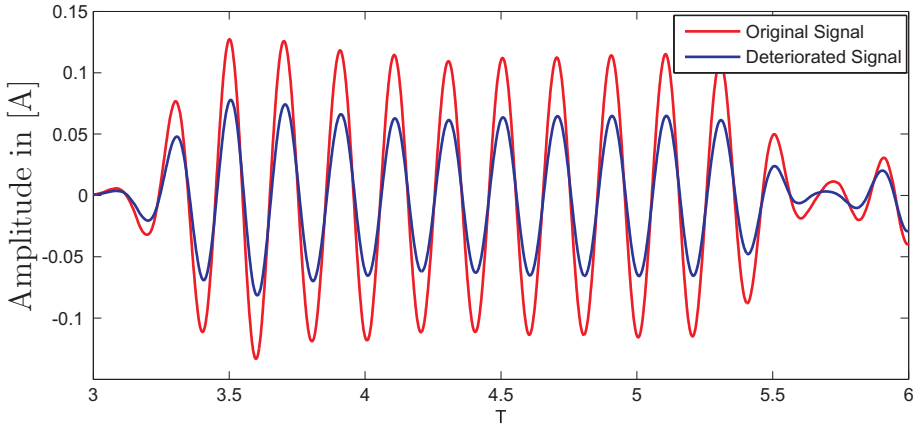

Figure 4.14: Original and Deteriorated Signal.

In conclusion, the two complete sets of measurements show that indeed the nonlinearity parameter in the HAZ is higher than in the base material and the weld. This corresponds well with the expectation that the damage level in the HAZ is higher than in the base material. On the other hand reliability issues are apparent. While all the measurements in the base material result in nonlinearity parameters similar to each other, the measurements in the HAZ show an elevated nonlinearity

only 4 out of 6 times. This has to be addressed either by improving the reliability of the measurement itself or changing the measurement pattern. Furthermore these measurements are not sufficient to correlate the elevated nonlinearity solely to creep damage. The heating of the material during the process of welding can cause changes in the microstructure and therefore might be the reason for the increase. Also there is no information about the change in nonlinearity in the base material compared to the virgin state.

4.3.2 Measurement on Annealed Specimen

A first step to gain more insight is taken by annealing this same creep damaged specimen. This process restores the microstructure of the specimen to a certain extent. The dislocation density decreases and micro-voids are annihilated. Measurements after the annealing show the correlation between dislocation/void density and the measured material nonlinearity. For the annealing, the specimen is heated to 1100°C for 2 hours in air followed by in-furnace cooling to room temperature in 12 hours. This heat treatment causes a strong oxidation of the specimen surface which therefore has to be polished prior to any measurements. As the custom transducers are not available for measurements anymore only the standard transducers are used to obtain the measurements. It is important to account for the reduction in thickness when calculation the nonlinearity parameter. The corrosion and polishing reduces the thickness of the sample to 6.6 mm from originally 7.2 mm. The measurements are taken along the middle line covering approximately the same spots as the first set of measurements. The positions are shown in Figure 4.15.

The resulting nonlinearity parameters compared to the measurements before the annealing are shown in Figure 4.16. Clearly, besides two points, the material nonlinearity measured after annealing is lower than before. This corresponds to the expected

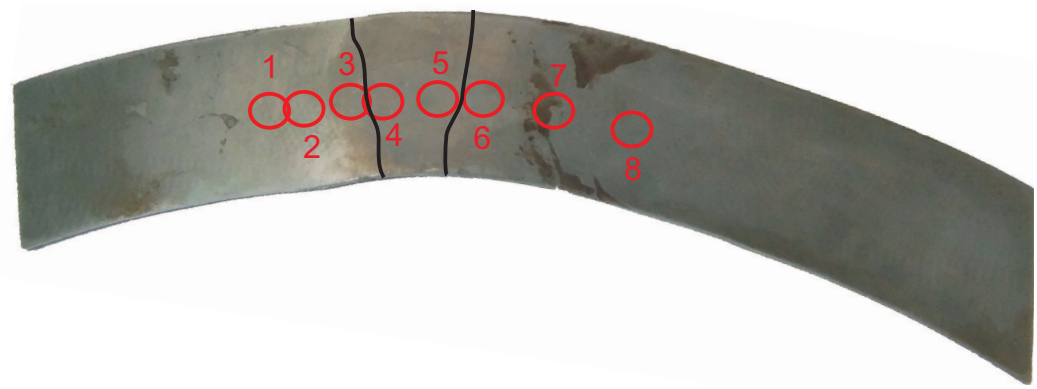

Figure 4.15: Position of Examined Points on the Specimen for Measurements after Annealing.

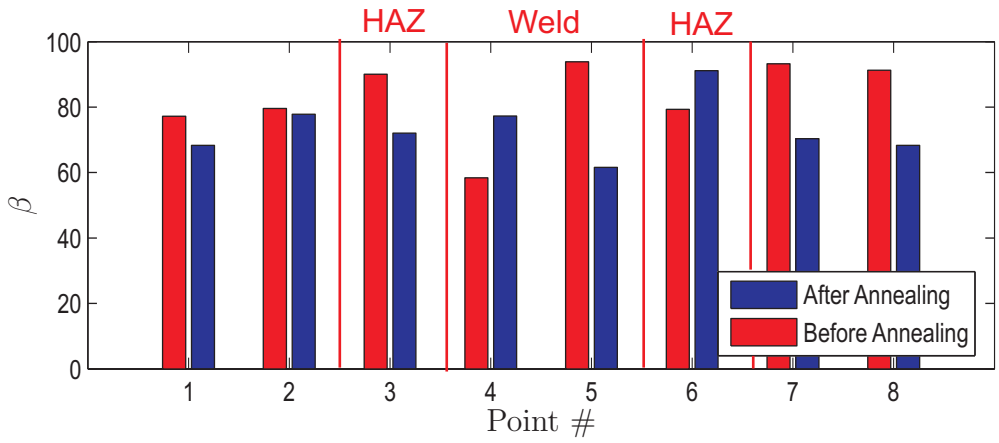

Figure 4.16: Material Nonlinearity before and after Annealing Compared.

behavior. The points that show the inverse trend might be due to different surface conditions. It is interesting to note that the peak of nonlinearity on the left side of the weld(in this measurement Point 3) disappeared. This could indicate that the elevated nonlinearity before the annealing was due to dislocations and voids possibly created by creep and then annihilated by the heat treatment. The peak on Point 5 seems to be reduced significantly as well, but as Point 6 of the measurement after annealing is at about the level of Point 5 before the annealing this might also indicate a slight inaccuracy in matching the points.

In conclusion, one can interpret that the generally lower level of nonlinearity after the annealing proves that the measurements can track changes in the microstructure. The strong decrease of nonlinearity at Point 4 suggests that the there was a high dislocation density in the HAZ. The decrease in Point 5 cannot be definitely connected to the heat treatment.

4.3.3 Nonlinearity Change by Welding

Strong heat can change the microstructure of steel. Therefore one has to investigate how much of the measured increase in nonlinearity is due to the heat from the welding process. Therefore measurements on an A36 steel specimen are done before and after welding it. For the experiment 3 measurements are taken on each strip before and after welding. The setup is equivalent to the one presented in the Experimental Setup chapter. The signal is a 5 MHz, 11 cycle toneburst with varying output level from 40 % to 95 % of the maximum output. The results of these measurements are shown in Figure 4.17. This figure shows that the nonlinearity is not changed significantly by the welding. The nonlinearities of single points are different before and after welding but there is no trend apparent and the differences are fairly small which means they only represent the normal scatter of a measurement. Therefore this experiment shows that the heat introduced by the welding process does not affect the material

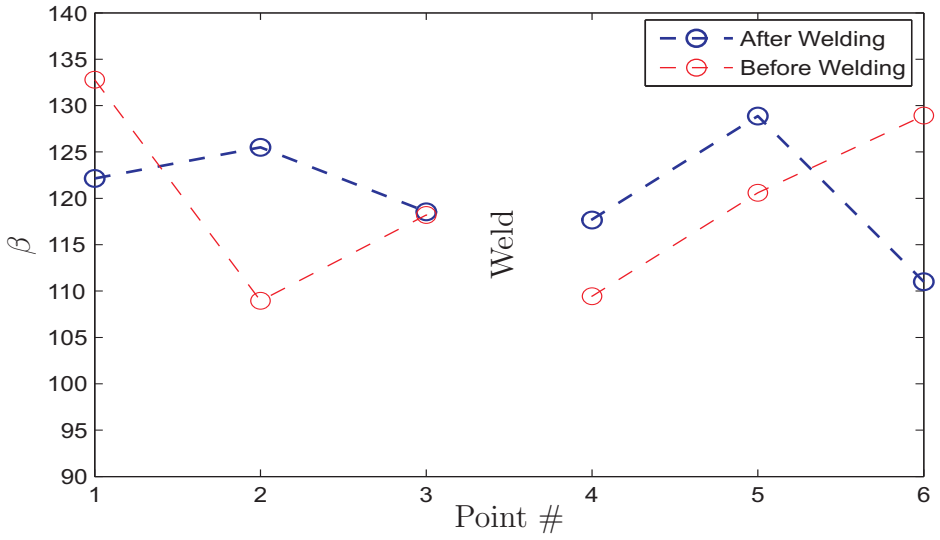

Figure 4.17: Material Nonlinearity before and after Welding.

nonlinearity significantly. Note that A335 steek has a different composition than A36 steel.

Therefore direct conclusions on the effect of heat on the nonlinearity parameter of A335 can hardly be drawn. However this experiment shows that an increase of nonlinearity as reaction to heat is not necessarily a characteristic of steel.

CHAPTER V

CONCLUSIONS AND OUTLOOK

This research develops a setup that can be used to obtain relative measurements of the acoustic nonlinearity parameter. Measurements on a welded steel pipe component show elevated nonlinearity in the HAZ according to the expected higher damage level in that area. Measurements after annealing and on a welded specimen without any damage suggest that the increase in nonlinearity in the HAZ is caused by creep damage.

The original goal to establish a setup that can reliably measure the absolute nonlinearity parameter is yet to be worked out. The measurements generally result in values that are too high. This means that even though extraneous sources of nonlinearity have been greatly reduced, some are still existing. Among them are the transducers and the couplant. While nonlinearity from the transducers can be reduced by different design, the couplant will always remain as a source of nonlinearity. The transducers used show different performances. With the standard transducers lower nonlinearities are measured while the custom transducers are more sensitive. In future work, the transducers and couplings need to be examined more thoroughly because they represent a main source of nonlinearity and consistency issues. Also different systems to generate and receive the signals should be considered. The results show some significant scatter from measurement to another. Even though a thorough statistical analysis is omitted in this project, it can be seen that the scatter is smaller than the expected change of nonlinearity in creep experiments.

The experiments on creep damaged specimen show significantly higher nonlinearity in the heat affected zone (HAZ) than in the base material. This indicates that the most creep damage is focused on the HAZ. It is shown that the technique is generally capable of detecting the elevated nonlinearity while there are also issues with reliability. To better correlate the data from the experiments future work has to include an examination of the microstructure of the specimen. Moreover the results from the measurements after annealing show that the nonlinear measurement detects changes of the micro-structure, that is decrease in nonlinearity in accordance with a reduced dislocation density by the annealing.

Additional measurements on A36 steel before and after welding do not show a considerable change in nonlinearity which suggests that the elevated nonlinearity parameter in the HAZ is in fact due to creep damage and not caused by the weld.

REFERENCES

[1] Achenbach, J., *Wave propagation in elastic solids*. North-Holland series in applied mathematics and mechanics, North-Holland Pub. Co., 1999.

[2] Baby, S., Kowmudi, B. N., Omprakash, C., Satyanarayana, D., Balasubramaniam, K., and Kumar, V., "Creep damage assessment in titanium alloy using a nonlinear ultrasonic technique," *Scripta Materialia*, vol. 59, no. 8, pp. 818 – 821, 2008.

[3] Barnard, D. J., "Variation of nonlinearity parameter at low fundamental amplitudes," *Applied Physics Letters*, vol. 74, no. 17, pp. 2447–2449, 1999.

[4] Bressers, J., *Creep and fatigue in high temperature alloys*. Applied Science Publishers, 1981.

[5] Cantrell, J. H., "Substructural organization, dislocation plasticity and harmonic generation in cyclically stressed wavy slip metals," *Proceedings of the Royal Society of London Series A-mathematical Physical and Engineering Sciences*, vol. 460, no. 2043, pp. 757–780, 2004.

[6] Dace, G. E., Thompson, R. B., Brasche, L. J. H., Rehbein, D. K., and Buck, O., "Nonlinear acoustics, a technique to determine microstructural changes in materials," in *Review of Progress in Quantitative Nondestructive Evaluation*, vol. 10, pp. 1685–1692, 1991.

[7] Dace, G. E., Thompson, R. B., and Buck, O., "Measurement of the acoustic harmonic generation for materials characterization using contact transducers," in *Review of Progress in Quantitative Nondestructive Evaluation. Vol. 11B* (D. O. Thompson & D. E. Chimenti, ed.), vol. 11, pp. 2069–2076, 1992.

[8] Hamilton, M. and Blackstock, D., *Nonlinear acoustics*. Academic Press, 1998.

[9] Horowitz, P. and Hill, W., *The art of electronics*. No. v. 816 in The Art of Electronics, Cambridge University Press, 1989.

[10] Kassner, M. E., *Fundamentals of creep in metals and alloys*. Amsterdam: Elsevier, 2nd ed. ed., 2009.

[11] Manson, S. S., *Fatigue and durability of metals at high temperatures*. Materials Park, Ohio: ASM International, 2009.

[12] Mueller, T., "Nonlinear ultrasonics: Signal processing considerations and a nonlinear parameter for rayleigh waves," Master's thesis, Georgia Institute of Technology, 2006.

[13] Ohtani, T., Kawashima, K., Drew, M., and Guagliard, P., "Nonlinear acoustic evaluation of creep damage in boiler heat exchange tubes," *Japanese Journal of Applied Physics*, vol. 46, no. 7b, pp. 4577–4582, 2007.

[14] Oppenheim, A., Schafer, R., and Buck, J., *Discrete-time signal processing*. Prentice-Hall signal processing series, Prentice Hall, 1999.

[15] Papadakis, E. P., "Correction for diffraction losses in the ultrasonic field of a piston source," 1959. journal article.

[16] Sittig, E., "Effects of Bonding and Electrode Layers in Transmission Parameters of Piezoelectric Transducers used in Ultrasonics Digital Delay Lines," *IEEE Transactions on Sonics and Ultrasonics*, vol. SU16, no. 1, pp. 2–&, 1969.

[17] Sposito, G., Ward, C., Cawley, P., Nagy, P., and Scruby, C., "A review of non-destructive techniques for the detection of creep damage in power plant steels," *NDT & E International*, vol. 43, no. 7, pp. 555 – 567, 2010.

[18] Thompson, R. B., Buck, O., and Thompson, D. O., "Higher harmonics of finite amplitude ultrasonic waves in solids," 1976. journal article.

[19] Valluri, J. S., Balasubramaniam, K., and Prakash, R. V., "Creep damage characterization using non-linear ultrasonic techniques," *ACTA MATERIALIA*, vol. 58, pp. 2079–2090, APR 2010.

[20] Waren, A., Onoe, M., and Coquin, G., " Determination of Elastic and Piezoelectric Constants for Crystals in Class (3M)," *Journal of the Acoustical Society of America*, vol. 42, no. 6, pp. 1223–&, 1967.

[21] Yost, W. T. and Cantrell, J. H., "Anomalous nonlinearity parameters of solids at low acoustic drive amplitudes," *Applied Physics Letters*, vol. 94, no. 2, 2009.

[22] Zhou, Q. F., Cannata, J., and Shung, K. K., "Design and modeling of inversion layer ultrasonic transducers using LiNbO3 single crystal," *ULTRASONICS*, vol. 44, pp. E607–E611, DEC 22 2006. Ultrasonics International (UI 05)/ World Congress on Ultrasonics (WCU 2005), Beijing, PEOPLES R CHINA, AUG 29-SEP 01, 2005.